Weierstraß-Institut
für Angewandte Analysis und Stochastik
Leibniz-Institut im Forschungsverbund Berlin e. V.

Preprint ISSN 2198-5855

Stochastic model for LFP-electrodes

Wolfgang Dreyer, Peter K. Friz, Paul Gajewski, Clemens Guhlke, Mario Maurelli

submitted: November 7, 2016

Weierstrass Institute
Mohrenstr. 39
10117 Berlin
Germany
E-Mail: wolfgang.dreyer@wias-berlin.de
peter.friz@wias-berlin.de
clemens.guhlke@wias-berlin.de
paul.gajewski@wias-berlin.de
mario.maurelli@wias-berlin.de

No. 2329
Berlin 2016

2010 *Mathematics Subject Classification.* 35Q84, 80A22, 74N30.

2010 *Physics and Astronomy Classification Scheme.* 05.10.Gg, 05.70.Fh, 05.70.Ce, 82.47.Aa.

Key words and phrases. lithium-ion batteries, lithium iron phospate, thermodynamics, phase transitions, many particle electode.

This research was supported by the Research Center MATHEON through project C-SE8 funded by the Einstein Center for Mathematics Berlin.

Edited by
Weierstraß-Institut für Angewandte Analysis und Stochastik (WIAS)
Leibniz-Institut im Forschungsverbund Berlin e. V.
Mohrenstraße 39
10117 Berlin
Germany

Fax: +49 30 20372-303
E-Mail: preprint@wias-berlin.de
World Wide Web: http://www.wias-berlin.de/

Abstract

In the framework of non-equilibrium thermodynamics we derive a new model for porous electrodes. The model is applied to $\mathrm{LiFePO_4}$ (LFP) electrodes consisting of many LFP particles of nanometer size. The phase transition from a lithium-poor to a lithium-rich phase within LFP electrodes is controlled by surface fluctuations leading to a system of stochastic differential equations.

The model is capable to derive an explicit relation between battery voltage and current that is controlled by thermodynamic state variables. This voltage-current relation reveals that in thin LFP electrodes lithium intercalation from the particle surfaces into the LFP particles is the principal rate limiting process. There are only two constant kinetic parameters in the model describing the intercalation rate and the fluctuation strength, respectively. The model correctly predicts several features of LFP electrodes, viz. the phase transition, the observed voltage plateaus, hysteresis and the rate limiting capacity. Moreover we study the impact of both the particle size distribution and the active surface area on the voltage-charge characteristics of the electrode. Finally we carefully discuss the phase transition for varying charging/discharging rates.

1 Introduction

In recent years there is increasing need for powerful and effective batteries due to rapidly growing electro mobility. Currently the most promising battery type are lithium-ion batteries. In the last decades big progress has been made in the development of both new electrode materials and new electrolytes. In order to properly apply and improve the existing materials and their combination a deep understanding of the materials constitutive properties is mandatory. To this end mathematical models embodying the physical and chemical behavior of battery materials from the micro to the macro scale are essential.

Atomistic models are needed to identify the relevant reaction and transport mechanisms. On the other hand the battery developer needs continuum models to effectively describe and predict the processes on the scale of battery cells. In particular only continuum models are capable to describe the interactions between macroscopic phenomena like heat and charge transport which are accompanied by mechanical deformations. Moreover, continuum models provide powerful tools to study the impact of these processes on battery voltage and currents.

Many classical continuum models for lithium-ion batteries rely on the framework that was developed by Newman et al. [DFN93, DN97, SN04]. Here diffusion processes within electrodes and electrolytes are described by simplified diffusion equations, and the transfer of charge is modeled by Butler-Volmer kinetics [Fra13, HSB11, SD11, FD11, FSP$^+$14]. For known model parameter, these models are capable to determine the influence of the battery geometry on

the cell voltage and thus configure a suitable battery design. Although the Newman models are quite popular they exhibit the following drawbacks:

1 The dependency of the model parameter on temperature, salt concentration, state of charge and geometry of the electrode are often unclear.

2 The microstructure of the electrode is included via empirical model parameter.

3 The incorporation of volume changes and elastic deformation is severely limited in Newman models.

Thus many experimental measurements of the parameter are necessary. These drawbacks imply a restricted applicability of Newman models.

More useful models are those where

1 the number of model parameter is as minimal as possible,

2 all model parameter must have a simple physical basis,

3 physical restrictions on the model parameter must be known.

These requirements are guaranteed if the battery model is embedded in non-equilibrium thermodynamics that discriminates between universal principle and the constitutive properties for the material at hand [MR59, dM63, Mül85, Bed86]. In this framework numerous phenomena can be consistently coupled. In particular, non-equilibrium thermodynamics is capable to construct a hierarchy of models on different levels of abstraction, ranging from models spatially resolving the electrodes until impedance models [Baz13, LZ11, LZ13, DGH11].

In this study we use non-equilibrium thermodynamics to develop a simple battery model with only a few constant(!) model parameter that comprises already a multitude of different phenomena. The model exemplarily describes the cathode material lithium iron phosphate (LFP). Modeling of LFP represents a challenge because during charging and discharging LFP exhibits a two-phase system with lithium-rich and lithium-poor phases [PNG97, DMC$^+$08, CEGS$^+$13]. The characteristic horizontal voltage plateaus in the voltage-capacity diagram is due to this phase transition, Figure 1_{right}. The task to design a model becomes ambitious here because the LFP electrode consists of an ensemble of nano-sized storage particles with the consequence that there are two different phase transition in competition [DJG$^+$10]: (i) There is a phase transition in the individual particles, and (ii) the ensemble of storage particles also shows a phase transition, where the particles consists with high and with low lithium filling, respectively. Moreover, the phase transition happens in a sequential order, in other words, the particles are filled according to the rule *one after the other* [DJG$^+$10]. Detailed studies of the phenomenon have revealed that the kind of phase transition depends on the charging speed and the size of the storage particles [LEGF$^+$14, LWG$^+$15, CEGS$^+$13].

Models for both kinds of phase transitions do already exist. The phase transition within a storage particle is usually described by a phase field model [ZB14, SCB08, BCB11]. Here the interface between a lithium-rich and a lithium-poor phase is spatially resolved. This kind of model allows a

detailed study of the interface motion in the particle. In particular, it is possible to investigate the influence of that motion to mechanical degradation of the particle [KR16]. Moreover, simulations on this level are quite involved and only possible for a few storage particles. There is a further drawback that is more serious than the problem of simulation capabilities. In fact, phase field models are able to represent the horizontal voltage plateaus. However, due to spinodal decomposition of the phases, which is an inherent property of any kind of phase field model, these models exhibit jumps of the battery voltage. This behavior is related to the fact that many phase field treatments do not physically judge the actual properties at the interface. Already such simple models as the Cahn-Hilliard model show inconsistencies here [DG15]. On the other hand careful experimental studies unambiguously show that the time scale of the phase transition within a nanosized particle happens is much smaller than the charging time of the battery cell. Thus on the time scale of charging the phase transition within the ensemble of storage particles is the dominant one [LML$^+$15].

The first model describing the phase transition within the ensemble was formulated by some of the current authors in [DJG$^+$10, DGH11]. Here so-called many-particle models are formulated, where the LFP electrode is described by an ensemble of communicating storage particles. These models are capable to correctly predict the inset of the phase transition during charging and they lead to the observed voltage-capacity plot with horizontal plateaus. In [DGH11] the mathematical setting consists of a single partial differential equation of Fokker-Planck type. This first model relies on some simplifications: i) There is no phase transition within the particles of the ensemble, i.e. in a LFP particle the lithium is homogeneously distributed, ii) the storage particles have equal size, iii) diffusion in the electrolyte, diffusion in the particles and diffusion along the surfaces of the particles have infinite mobilities, and iv) Adsorption processes and surface reactions on the particles have also infinite mobilities. However, these assumptions strongly restrict the applicability of a many-particle model that is based on a single Fokker-Planck equation. On the other hand, to remove those assumptions an extension of the Fokker-Planck setting would lead to a coupled system of Fokker-Planck equation. Its treatment is cumbersome and perhaps not possible at all.

For this reason in this paper we introduce a new many-particle model that does not rely on the above assumptions and which is fully developed within non-equilibrium thermodynamics. In particular, the LFP electrode is represented by a system of stochastic differential equations. It can be shown that under suitable assumptions including those from above the new stochastic model is then equivalent to the Fokker-Planck model. Despite its simplicity the stochastic model embodies already many properties of LFP electrodes. In particular we may predict the influence of the size distribution of the storage particles on the battery voltage.

The paper is organized as follows. We start in Section 2 with a phenomenological description of the functionality of a battery consisting of a LFP electrode as cathode and a metallic lithium electrode as anode. The stochastic model is introduced in Section 3. In Section 4 we discuss the relation between the phase transition and the battery voltage on the basis of a variety of simulations. The detailed derivation of the model including a list of model assumptions is the content of Section 5.

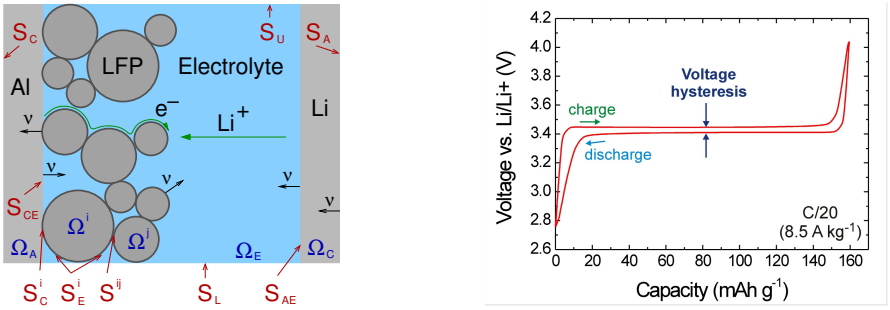

Figure 1: Left: Sketch of the LFP battery, Right: Typical voltage-capacity profile for a LFP electrode at low charging/discharging rate C/20 (Fig. 2 from [DJG$^+$10])

2 Description of the battery

Design of the battery. We consider a battery consisting of a LFP many-particle cathode, a liquid electrolyte and metallic lithium as the anode. The many-particle electrode consists of carbon coated LFP particles. The carbon coating improves the electric conductivity of the LFP particles [MDCK$^+$07, DBG$^+$05]. Usually carbon black is added to the LFP electrode such that the particles are electrically connected to each other. We neglect the carbon black and model the electron transport by the assumption that carbon coated LFP particles form an electric network. Thus the electron transport is achieved along the carbon coated particle surfaces. Moreover some LFP-particles are attached to a metal based current collector. Here usually aluminum is utilized. The electrolyte is a mixture of some lithium salt dissolved in some liquid organic solvent, e.g. LiPF_6 dissolved in a mixture of ethylene and dimethyl carbonate. The passive components of the battery such as binder, separator and further additives are ignored in this study. A sketch of the battery is shown in Figure 1.

Processes within the battery. During discharging of the battery lithium is transferred from the lithium anode to the LFP many particle cathode and vice versa for the charging process. The transport of lithium is the main limiting phenomenon that controls the functionality of the battery. The transport process itself consists of a combination of several rate limiting phenomena. In particular, we have to distinguish between surface and bulk transport.

The main bulk phenomena are ion diffusion within the liquid electrolyte and lithium diffusion and phase separation within the LFP particles.

At the particle surface we have: i) tangential mass transport, in particular electron transport, ii) adsorption of electrolytic species, iii) an electron transfer reaction of the form $\mathrm{Li}^+ + \mathrm{e}^- \rightleftharpoons \mathrm{Li}$, and iv) the intercalation of lithium into the iron-phosphate lattice.

At the lithium anode the situation is more simple. Lithium is deposited on or dissolved from the electrode surface for the charging and the discharging process, respectively.

Further processes such as heat generation and transport, mechanical deformation, dendrite growth or aging processes are not among the topics of this work. However, the thermodynamic approach of Sect. 5 can be used to incorporate these phenomena as well.

Model restrictions. In this work we introduce a LFP battery model which describes the experimentally observed features of the battery and is easy to solve. Therefore we must restrict the full thermodynamic model of Sect. 5 by some simplifying assumptions. The main assumptions are:

- Large porosity of the LFP electrode and whose thickness is in the micro meter scale.
- Nano-sized LFP particles.
- Rigid LFP particles, i.e. volume and surface of a particle do not change for a varying charging state.
- Constant temperature due to high heat conduction, which is appropriate in small cells.
- Lithium is exclusively stored in the LFP particles and in the lithium anode.
- The lithium anode is equipped with a large surface.
- Fast surface diffusion.

The full and a more detailed list of assumptions can be found in Sect. 5.

In either case these assumptions allow the applicability of our model to micro batteries and/or to high power batteries. However, in the case of moderate charging-discharging times there is a much larger class of batteries where the assumption are appropriate.

3 The many-particle electrode model

In this section we introduce the many-particle model for a lithium ion battery as described above. The model consists of (i) a system of stochastic differential equations (SDE), (ii) a constraint prescribing the state of charge of the battery, and (iii) voltage and current relations. In the following we describe the main ingredients of the battery model. The detailed derivation of the model is postponed to Sect. 5.

Notations. The many-particle electrode consists of $N_{\mathtt{P}}$ storage particles indexed by $i = 1, 2, ..., N_{\mathtt{P}}$. The particles have volumes V^i and active surface areas $A^i_{\mathtt{E}}$, which are time independent due to the model assumption. The total volume and the total active surface area of the LFP particles are denoted by

$$V_{\mathtt{P}} = \sum_{i=1}^{N_{\mathtt{P}}} V^i \qquad \text{and} \qquad A_{\mathtt{E}} = \sum_{i=1}^{N_{\mathtt{P}}} A^i_{\mathtt{E}} \,. \tag{1}$$

The surface area of the lithium anode electrolyte interface is denoted by $A_{\mathtt{AE}}$.

Thermodynamic state. The number of stored lithium atoms in particle P_i at time $t \geq 0$ is denoted by $\mathcal{N}^i_{\mathrm{Li}}(t)$. The number of $\mathrm{FePO_4}$ units forming the matrix lattice of particle P_i is time independent and denoted by $\mathcal{N}^i_{\mathrm{FePO_4}}$. Each particle has the same time independent number density $n_{\mathrm{FePO_4}}$. The number densities of the intercalated lithium n^i_{Li} are time dependent but constant in space. The number densities are related to the number of stored lithium and to the number of $\mathrm{FePO_4}$ units by $\mathcal{N}^i(t) = n^i_{\mathrm{Li}}(t)V^i$ and $\mathcal{N}^i_{\mathrm{FePO_4}} = n_{\mathrm{FePO_4}}V^i$.

Each $\mathrm{FePO_4}$ unit provides a free lattice site that may be occupied by a lithium atom. Then the *mole fraction* $y^i \in [0,1]$ of occupied lattice sites of particle P_i is defined as

$$y^i(t) = \frac{n^i_{\mathrm{Li}}(t)}{n_{\mathrm{FePO_4}}} \,. \tag{2}$$

The thermodynamic state of the many-particle electrode is exclusively represented by the lithium mole fractions of the particles, $(y^i)_{i=1,2,\ldots,N_{\mathrm{P}}}$.

3.1 The deterministic model for the many particle electrode

The evolution of the thermodynamic state of the many-particle electrode is described by the ODE system

$$\frac{dy^i}{dt} = \frac{1}{\tau^i}\frac{m_{\mathrm{Li}}}{k_B T}(\mu_{s,\mathrm{Li}} - \mu_{\mathrm{Li}}(y^i)) \qquad \text{with} \quad \frac{1}{\tau^i} = \frac{k_{\mathrm{Li}}}{m_{\mathrm{Li}} n_{\mathrm{FePO_4}}}\frac{A^i_{\mathrm{E}}}{V^i} \,. \tag{3}$$

As shown in Sect. 5 the system (3) relies on mass balance equations of the stored lithium in the LFP particles. The right hand site of (3) arises from the desorption flux j^i_{Li} describing the intercalation of lithium atoms from the surface of particle P_i into the $\mathrm{FePO_4}$ lattice,

$$j^i_{\mathrm{Li}} = k_{\mathrm{Li}}\frac{m_{\mathrm{Li}}}{k_B T}\big(\mu_{\mathrm{Li}}(y^i) - \mu_{s,\mathrm{Li}}\big) \,. \tag{4}$$

The lithium flux is driven by the chemical potential difference $\mu_{\mathrm{Li}}(y^i) - \mu_{s,\mathrm{Li}}$, where $\mu_{s,\mathrm{Li}}$ represents the surface chemical potential of freely moving lithium on the particle surface and μ_{Li} is the chemical potential of $\mathrm{Li_yFePO_4}$, i.e. of intercalated lithium. The kinetic parameter k_{Li} has the unit kg/(m^{2}s) and represents the (constant) rate of intercalation of lithium atoms into the $\mathrm{FePO_4}$ lattice.

The assumption of fast surface diffusion implies that the surface chemical potential $\mu_{s,\mathrm{Li}}$ is the same for all LFP particles. The chemical potential of intercalated lithium, μ_{Li}, is a function of the lithium mole fraction y^i of the corresponding LFP particle. In order to model the phase separating behavior of $\mathrm{Li_yFePO_4}$, [SCB08, BCB11, DGH11], we choose the widely used non-monotone function

$$\mu_{\mathrm{Li}} = \mu^{\mathrm{ref}}_{\mathrm{Li}} + \tfrac{L}{m_{\mathrm{Li}}}(1-2y) + \tfrac{k_B T}{m_{\mathrm{Li}}}\ln\left(\frac{y}{1-y}\right) \,. \tag{5}$$

The chemical potential consists of three contributions. The first part $\mu^{\mathrm{ref}}_{\mathrm{Li}}$ is a constant material parameter depending on the properties of $\mathrm{Li_yFePO_4}$. The second part is an energetic contribution, where L has the unit J (Joule) and denotes the heat of solution. The constant quantity L

controls the energy barrier between the lithium-poor and the lithium-rich phase. Finally there is a third contribution that takes into account the entropy of mixing of lithium atoms on the available lattice sites. Figure 2 depicts the chemical potential function $\mu_{\mathrm{Li}}(y) - \mu_{\mathrm{Li}}^{\mathrm{ref}}$ for a typical choice of $L = 94.4 \times 10^{-22}$ J.

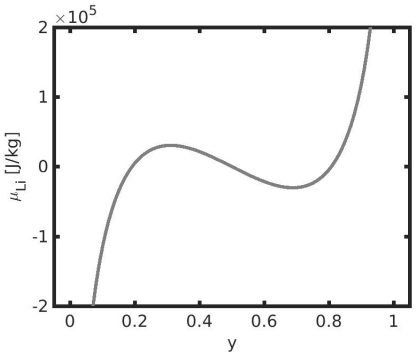

Figure 2: Non-monotone chemical potential of lithium in iron-phosphate.

State of charge - charging rate. The *total mole fraction* $q \in [0,1]$ of the many-particle ensemble describes the *state of charge* of the battery,

$$q(t) = \frac{\sum_{i=1}^{N_{\mathrm{P}}} \mathcal{N}_{\mathrm{Li}}^i(t)}{\sum_{j=1}^{N_{\mathrm{P}}} \mathcal{N}_{\mathrm{FePO_4}}^j} = \sum_{i=1}^{N_{\mathrm{P}}} \frac{V^i}{V_{\mathrm{P}}} y^i(t) \,. \tag{6}$$

The battery is fully charged for $q = 0$ and the state $q = 1$ corresponds to a fully discharged battery. The *charging rate* of the battery is given by the time derivative of the total mole fraction.

We assume that lithium can be stored exclusively in the LFP particles and not elsewhere. Thus in a galvanostatic charging/discharging process the total mole fraction q is the external control parameter. Consequently, the equation (6) represents a constraint on the evolution of the lithium mole fractions $y^1(t), y^2(t), ..., y^{N_{\mathrm{P}}}(t)$. According to (3) and (6) we have

$$\frac{dq}{dt} = \frac{m_{\mathrm{Li}}}{k_B T} \sum_{i=1}^{N_{\mathrm{P}}} \frac{V^i}{V_{\mathrm{P}}} \frac{1}{\tau_{\mathrm{Li}}^i} \big(\mu_{s,\mathrm{Li}} - \mu_{\mathrm{Li}}(y^i)\big) \,. \tag{7}$$

Then this equation must be used to determine the surface chemical potential $\mu_{s,\mathrm{Li}}$. In this context $\mu_{s,\mathrm{Li}}$ may be interpreted as a Lagrange multiplier. See also the analogue situation in Sect. 3.4 where the Fokker-Planck model of the many-particle electrode is described.

Electric current. There is a universal relation between the charging rate $d_t q$ of the LFP particles and the electric current I which flows through the battery,

$$I = e_0 n_{\mathrm{FePO_4}} V_{\mathrm{P}} \frac{dq}{dt} \,. \tag{8}$$

Here the physical unit of I is A (Ampere). The relation (8) will be derived in Section 5. It relies on bulk and surface mass balance equations.

Battery voltage. The battery voltage U is defined as the electric potential difference between cathode and anode. Based on the constitutive relations of Sect. 5 we obtain the relation

$$U = U^{\text{ref}} - \frac{m_{\text{Li}}}{e_0} \sum_{i=1}^{N_{\text{P}}} \frac{A_{\text{E}}^i}{A_{\text{E}}} \big(\mu_{\text{Li}}(y^i) - \mu_{\text{Li}}^{\text{ref}}\big) - \frac{k_B T}{e_0} \Big(\frac{1}{A_{\text{E}} j_{\text{P}}} + \frac{1}{A_{\text{A}} j_{\text{A}}} \Big) I. \tag{9}$$

The total exchange currents corresponding to the LFP particles and the lithium anode, respectively, are constants and they are defined as

$$\frac{1}{j_{\text{P}}} = \Big(\frac{1}{j_{\text{ic}}^{\text{P}}} + \frac{1}{j_{\text{ad}}^{\text{P}}} + \frac{1}{j_{\text{re}}^{\text{P}}} \Big) \qquad \text{and} \qquad \frac{1}{j_{\text{A}}} = \Big(\frac{1}{j_{\text{ad}}^{\text{A}}} + \frac{1}{j_{\text{de}}^{\text{A}}} \Big) \,. \tag{10}$$

The battery voltage consists of three contributions:

1 The first contribution is a constant voltage $U^{\text{ref}} = \frac{1}{e_0}(m_{\text{e}^-}\mu_{\text{e}^-}|_{S_{\text{C}}} + m_{\text{Li}^+}\mu_{\text{Li}^+}|_{S_{\text{A}}} - m_{\text{Li}}\mu_{\text{Li}}^{\text{ref}})$ characterizing the current collector of the cathode, the lithium anode and the LFP particles.

2 The second contribution is time dependent and depends on the intercalation process within the LFP many particle electrode. It nonlinearly depends on the electric current I via the mole fractions y^i.

3 The third contribution is linear in I and describes five different interfacial dissipative mechanisms. We have five constant material parameter due to lithium intercalation, j_{ic}^{P}, surface reaction, j_{re}^{P}, adsorption at the LFP particles, j_{ad}^{P}, adsorption at the lithium anode, j_{ad}^{A}, and lithium deposition at the anode, j_{de}^{A}. The parameter j_{ic}^{P} is related to the intercalation rate k_{Li} by

$$j_{\text{ic}}^{\text{P}} = \frac{e_0}{m_{\text{Li}}} k_{\text{Li}} \,. \tag{11}$$

The linearity of the third contribution results from linear flux-driving force constitutive laws for adsorption, reaction and intercalation processes. It is easy to extend the model by corresponding nonlinear constitutive equations of Butler-Volmer type [DGM15, DGM16]. In this case we would obtain logarithmic voltage-current relations.

3.2 The stochastic model for the many-particle electrode

In this section we extend the ODE model of the last paragraph by adding some noise. The noise may be understood as small fluctuations occurring during the intercalation process.

To this end we assume that the lithium mole fractions $y^1, y^2, ..., y^{N_{\text{P}}}$ represent possible values of a vector-valued random variable $\boldsymbol{Y} = (Y^1, Y^2, ..., Y^{N_{\text{P}}})$.

The set $\{\boldsymbol{Y}(t) |\, t \geq 0\}$ defines a stochastic process that is determined by the SDE system

$$\begin{aligned} Y^i(t) - Y^i(t_0) = & \frac{1}{\tau^i} \frac{m_{\text{Li}}}{k_B T} \int_{t_0}^{t} \big(\mu_{s,\text{Li}}(s) - \mu_{\text{Li}}(Y^i(s)) \big) \, ds \\ & + \nu^i \sqrt{\frac{2}{\tau^i}} \big(W^i(t) - W^i(t_0) \big) - \frac{1}{\tau^i} \big(Z(t) - Z(t_0) \big) \,. \end{aligned} \tag{12}$$

With respect to the deterministic system described above, we have the following differences:

- The difference $W^i(t) - W^i(t_0)$ represents the increment of a Wiener process which models small lithium fluctuations on the surface of the particles. All W^i are independent processes. The strength of the noise is controlled by the constant parameter ν_0 which is related to ν^i by

$$\nu^i = \frac{\nu_0}{\sqrt{V^i}} \,. \tag{13}$$

- The difference $Z(t) - Z(t_0)$ is introduced to obtain a relation for the chemical potential $\mu_{s,\mathrm{Li}}$ which corresponds to (7) in the deterministic setting: without the term Z, the formula for $\mu_{s,\mathrm{Li}}$ would contain the white noise term $\dot{W}^i$ which is infinite.

From a thermodynamic point of view the fluctuations are introduced by a modification of the lithium flux j_{Li}. Later on in Sect. 5.5 we show that this modification is consistent with the 2nd law of thermodynamics, i.e. the extended lithium flux guarantees a non-negative entropy production as well.

The Wiener process (or Brownian motion) $W = W(t,\omega)$ is a particular stochastic process, which is, roughly speaking, a random function of time. The Wiener process is the process whose time increments are independent, i.e., for any $r < s < t$, $W(s) - W(r)$ and $W(t) - W(s)$ are independent, and have Gaussian probability law, with mean 0 and variance given by the time increment, i.e. $W(t) - W(s)$ has the law $\mathcal{N}(0, t-s)$. The Wiener process is characterized as the process whose (distributional) time derivative is the white noise in one dimension. More details are given in Section 5.9.

State of charge. As in the deterministic case the state of charge is given by the total mole fraction q defined as

$$q(t) = \sum_{i=1}^{N_{\mathrm{P}}} \frac{V^i}{V_{\mathrm{P}}} Y^i(t) \,. \tag{14}$$

In the galvanostatic regime the function q is given and leads to a constraint on the mole fractions. The surface chemical potential $\mu_{s,\mathrm{Li}}$ can here be interpreted as a Lagrange multiplier, which has to be chosen such that the constraint (14) is satisfied. To obtain a similar relation for the surface chemical potential $\mu_{s,\mathrm{Li}}$ as in the deterministic case, we define the function Z as

$$Z(t) = \frac{\sum_{i=1}^{N_{\mathrm{P}}} \frac{V^i}{V_{\mathrm{P}}} \nu^i \sqrt{\frac{2}{\tau^i}} W^i(t)}{\sum_{j=1}^{N_{\mathrm{P}}} \frac{V^j}{V_{\mathrm{P}} \tau^j}} \,. \tag{15}$$

Note that Z is a Gaussian process with covariance $\left(\sum_{i=1}^{N_{\mathrm{P}}} (\frac{V^i}{V_{\mathrm{P}}} \nu^i)^2 \frac{2}{\tau^i}\right) / \left(\sum_{j=1}^{N_{\mathrm{P}}} \frac{V^j}{V_{\mathrm{P}} \tau^j}\right)^2$, which is infinitesimal for N_{P} large.

Finally the SDE system (12) and the constraint (14) imply an explicit relation for the surface chemical potential $\mu_{s,\mathrm{Li}}$,

$$\frac{dq}{dt} = \frac{m_{\mathrm{Li}}}{k_B T} \sum_{i=1}^{N_{\mathrm{P}}} \frac{V^i}{V_{\mathrm{P}}} \frac{1}{\tau^i_{\mathrm{Li}}} \big(\mu_{s,\mathrm{Li}}(t) - \mu_{\mathrm{Li}}(Y^i(t))\big) \,. \tag{16}$$

After inserting this relation into the SDE (12), we see that the particles are interacting through the term $\mu_{s,\mathrm{Li}}$.

Electric current. The relation (8) between the electric current and the total mole fraction is derived from general balance equations without using any constitutive equations. Therefore the relation (8) holds also in the stochastic case,

$$I = e_0 n_{\mathrm{FePO}_4} V_{\mathtt{P}} \frac{dq}{dt} \,. \tag{17}$$

Battery voltage. The derivation of the battery voltage results from the constitutive equation, in particular from the constitutive equation of the lithium flux j_{Li} which depends on the Wiener process. However, we will show in Section 5 that the same relation holds as in the deterministic setting, i.e.

$$U = U^{\mathsf{ref}} - \tfrac{m_{\mathrm{Li}}}{e_0} \sum_{i=1}^{N_{\mathtt{P}}} \tfrac{A_{\mathtt{E}}^i}{A_{\mathtt{E}}} \big(\mu_{\mathrm{Li}}(Y^i) - \mu_{\mathrm{Li}}^{\mathsf{ref}}\big) - \tfrac{k_B T}{e_0} \Big(\frac{1}{A_{\mathtt{E}} j_{\mathtt{P}}} + \frac{1}{A_{\mathtt{A}} j_{\mathtt{A}}} \Big) I. \tag{18}$$

3.3 Some features of the many particle electrode model

Both the deterministic model and the stochastic model are thermodynamically consistent. In other words, both models are fully derived in the context of non-equilibrium thermodynamics. Concerning the stochastic model this is a remarkable feature, because up to now there was no possibility to apply non-equilibrium thermodynamics [MR59, dM63, Mül85] on a scale where stochastic fluctuation can be observed. For the first time we found that stochastic elements can be introduced within surface thermodynamics but not within non-equilibrium thermodynamics of the bulk. This fact fits to the observation that stochastic effects are more likely to influence surface phenomena rather than bulk phenomena. A prominent example concerns nucleation processes.

Our assumptions from Section 2 reduce the relevant kinetic phenomena to pure surface phenomena. For this reason we are able to embody the complex charging-discharging process of a LFP battery in a model of remarkable simplicity with only few phenomenological parameter. For example, the dynamics of the many-particle electrode is only controlled by the intercalation rate k_{Li} and the strength of the stochastic fluctuations ν_0. Consequently the experimental determination of the two parameter is an easy task.

In contrast, the battery voltage, see (9) and (18), is controlled by further parameters, viz. the constant exchange currents $j_{\mathtt{P}}$ and $j_{\mathtt{A}}$. Both parameter produce an observable shift of the voltage plateau in the voltage-current diagram if the charge current is changed [SD11]. This shift is clearly depicted by Figure 13.

Moreover Figure 13 shows the effect of a rate limiting battery capacity. An increase of the charge current apparently decreases the maximal possible state of charge. This phenomenon emerges from the appearance of non-monotone chemical potentials of the LFP particles. Numerical simulations in Sect. 4 impressively confirm this observation.

3.4 Stochastic model in the Fokker-Planck setting

It is possible to associate the system of SDEs to a family of Fokker-Planck equations, which give an equivalent description of the SDE system in the limit of large number of particles.

To understand the link between SDEs and Fokker-Planck equations, we start by recalling the following well-known fact [Szn91]: given a drift b, a number σ and a Wiener process W, if a real-valued stochastic process Y satisfies the SDE

$$Y(t) = Y(t_0) + \int_{t_0}^{t} b(s, Y(s))\, ds + \sigma(W(t) - W(t_0)), \tag{19}$$

then, for every $t > 0$, the probability law of Y admits a density $p(t, \cdot)$ which satisfies the Fokker-Planck equation

$$\partial_t p(t, y) = -\partial_y(b(t, y)p(t, x)) + \frac{\sigma^2}{2}\partial_y^2 p(t, y)\ . \tag{20}$$

Now we consider the case of single size particles. Here we will ignore both the Z term in (12), and the boundary conditions $Y^i \in (0, 1)$. We suppose for a moment that the chemical potential $\mu_{s,\mathrm{Li}}$ do not depend on the particle number N_P nor on the specific realization of the noise. Then all particles would be identically distributed, i.e. they have the same probability law, and would behave independently. Then the system of SDEs (12) with (16) would converge, in a suitable sense, to the single Fokker-Planck equation, viz.

$$\partial_t p(t, y) = \frac{1}{\tau}\frac{m_\mathrm{Li}}{k_B T}\partial_y\big((\mu_\mathrm{Li}(y) - \mu_{s,\mathrm{Li}}(t))p(t, y)\big) + \frac{\nu^2}{\tau}\partial_y^2 p(t, y)\ , \tag{21}$$

where $\mu_{s,\mathrm{Li}}$ is given by

$$\mu_{s,\mathrm{Li}}(t) = \tau\frac{k_B T}{m_\mathrm{Li}}\frac{dq}{dt} + \int_{-\infty}^{\infty} \mu_\mathrm{Li}(y)\, p(t, y)\, dy\ . \tag{22}$$

The main point here for the SDE system (12), and more general for mean field SDEs, is that this convergence remains true, even if the particle are interacting, since $\mu_{s,\mathrm{Li}}$ is not fixed. Therefore, in the case of single size particles, this Fokker-Planck equation can be used for our model in the limit of large number of particles.

This Fokker-Planck equation is identical to the Fokker-Planck equation in [DGH11] for a LFP many particle electrode. In [DGH11] a statistical approach is used to derive the Fokker-Planck equation. Existence and uniqueness of the Fokker-Planck equation is proved in [DHM$^+$15] and a detailed discussion of the different time regimes can be found in [HNV12, HNV14]. It is shown in [DGH11] that the Fokker-Planck equation (21) is capable to predict and explain the voltage-capacity diagram and the phase transition within the many particle system. But the Fokker-Planck equation and the model approach of [DGH11] has two import drawbacks: Firstly the Fokker-Planck equation is difficult to extend to systems with different particle sizes and to include phenomena like charge transport in the electrolyte and heat transport. Secondly a precise physical interpretation of the parameter τ and ν is missing. Both drawbacks are fully removed by the approach of this paper. In Sect. 5 the stochastic model is fully derived in the context of

non-equilibrium thermodynamics and all quantities have a physical interpretation. In particular, in [DGH11] a Lagrange multiplier Λ was introduced to satisfy the constraint (14) which reads in the Fokker-Planck setting for identical particle sizes

$$q(t) = \int_{-\infty}^{\infty} y\, p(t,y)\, dy\ . \tag{23}$$

The derivation of the SDE system yields that the Lagrange multiplier is the surface chemical potential of lithium, i.e. $\Lambda = \mu_{s,\mathrm{Li}}$. Moreover, in [DGH11] the coefficient τ was interpreted as the relaxation time of the many particle system, however, dependence on the particle size was missing in [DGH11]. Here we can show that τ is related to the intercalation process of lithium into the iron phosphate lattice and how τ is related to the particle size.

In the case of different size particles, the particles are no more identically distributed, since small particles behave differently from large ones. However, the convergence result remains true, provided we replace the single Fokker-Planck equation (21) by a family of Fokker-Planck equations, parametrized by the radii R of the particles and coupled via the potential $\mu_{s,\mathrm{Li}}$, namely

$$\partial_t p(t,y,R) = \frac{1}{\tau(R)}\frac{m_{\mathrm{Li}}}{k_B T}\partial_y\big((\mu_{\mathrm{Li}}(y) - \mu_{s,\mathrm{Li}})p(t,y,R)\big) + \frac{\nu(R)^2}{\tau(R)}\partial_y^2 p(t,y,R)\ , \tag{24}$$

where now $\mu_{s,\mathrm{Li}}$ is given by

$$\mu_{s,\mathrm{Li}} = \frac{V_{\mathrm{P}}\frac{dq}{dt} + \int\int \mu_{\mathrm{Li}}(y)\,\frac{V(R)}{\tau(R)}\,p(t,y,R)\,dydR}{\int \frac{V(R)}{\tau(R)}\,\rho(R)\,dR}\ , \tag{25}$$

$V(R)$ is the volume of the particle of radius R, and $\tau(R)$ and $\nu(R)$ are suitable functions of the radius. This can be shown for example by a randomization procedure, see [FHM14]. In a second paper we prove rigorously this convergence in the different size case and with boundary conditions [DFG$^+$16].

3.5 Discussion and choice of model parameter

There are three kinds of distinguished model parameter. In fact in our model we have energetic parameter, kinetic parameter and structural parameter. Their meaning and selected values will be now discussed.

Energetic parameter. There are three energetic parameter in the various chemical potentials of the battery model. The chemical potential μ_{Li} of the LFP particles contains the parameter L representing the heat of solution. The parameter L controls the height of the energy barrier between the lithium-rich and the lithium-poor phase. For LFP the parameter has to be chosen such that the chemical potential μ_{Li} becomes non-monotone allowing phase separation. A typical value for L is

$$L = 94.4 \times 10^{-22}\mathrm{J}\ . \tag{26}$$

A further energetic parameter is the constant reference voltage U^{ref}. Its value depends on the material properties of both the LFP many-particle electrode and the lithium anode and can be read off from a volt-capacity diagram. A typical value is

$$U^{\text{ref}} = 3.4\text{V} \ . \tag{27}$$

The third parameter ν_0 controls the intensity of the fluctuation at the particle surfaces. For the Fokker-Planck setting a suitable choice of ν_0 is derived in [DGH11],

$$\nu_0 = \sqrt{\frac{k_B T}{L n_{\text{FePO}_4}}} \approx 10^{-15} \text{m}^{\frac{3}{2}} \tag{28}$$

Kinetic parameters. Our constitutive model embodies five distinguished kinetic mechanisms with dissipation. Each mechanism is controlled by a corresponding mobility coefficient. It is convenient to write the mobilities in the form of exchange currents.

$j_{\text{ic}}^{\mathtt{P}}$	lithium intercalation
$j_{\text{re}}^{\mathtt{P}}$	surface reaction
$j_{\text{ad}}^{\mathtt{P}}$	adsorption at the LFP particles
$j_{\text{ad}}^{\mathtt{A}}$	adsorption at the lithium anode
$j_{\text{de}}^{\mathtt{A}}$	deposition of lithium at the anode .

The kinetic parameter are either determined from atomistic theories or they can be read off from measurements. However, measurements with LFP particles of nano-size are difficult due to the phase transition in LFP. Moreover, the interaction of different surface processes and the experimental handling of composite electrodes bring further complexities.

In particular only a measurement of the total exchange currents $j_{\mathtt{P}}$ and $j_{\mathtt{A}}$ of the cathode and the anode are available in the literature, which appears in our model as the combinations (10) of the kinetic parameter. However, values for $j_{\mathtt{P}}$ differ by several orders of magnitude. Values for $j_{\mathtt{P}}$ in LFP which range from 10^{-6} A m^{-2} to 10^{-1} A m^{-2} are reported [LEGF$^+$14]. In this study we assume that the rate limiting process in the cathode is the lithium intercalation, i.e both lithium adsorption and electron transfer reaction are fast compared to the intercalation process,

$$j_{\text{ic}}^{\mathtt{P}} \ll j_{\text{re}}^{\mathtt{P}}, j_{\text{ad}}^{\mathtt{P}} \qquad \Longrightarrow \qquad j_{\mathtt{P}} \approx j_{\text{ic}}^{\mathtt{P}} \ . \tag{29}$$

For the numerical investigations we choose the value

$$j_{\text{ic}}^{\mathtt{P}} \approx j_{\mathtt{P}} = 0.15 \tfrac{\text{A}}{\text{m}^2} \ . \tag{30}$$

According to (11) the kinetic coefficient k_{Li} for the lithium intercalation is

$$k_{\text{Li}} = \tfrac{m_{\text{Li}}}{e_0} j_{\text{ic}}^{\mathtt{P}} = 10^8 \tfrac{\text{kg}}{\text{m}^2\text{s}} \ . \tag{31}$$

The exchange current $j_{\mathtt{A}}$ describes lithium ion adsorption and lithium deposition at the anode. Assuming that the adsorption process at the lithium metal electrode has no significant impact on the battery voltage, we state

$$A_{\mathtt{P}} j_{\mathtt{P}} \ll A_{\mathtt{AE}} j_{\mathtt{A}} \ . \tag{32}$$

According to these assumptions the voltage-current relation (9) for the deterministic model simplifies to

$$U = U^{\text{ref}} - \frac{m_{\text{Li}}}{e_0} \sum_{i=1}^{N_{\text{P}}} \frac{A_{\text{E}}^i}{A_{\text{E}}} \big(\mu_{\text{Li}}(y^i) - \mu_{\text{Li}}^{\text{ref}}\big) + \frac{m_{\text{Li}}}{e_0} \frac{k_B T}{e_0} \frac{1}{A_{\text{E}} k_{\text{Li}}} I \,. \tag{33}$$

The voltage-current relation (18) for the stochastic simplifies correspondingly.

Structural parameters. There are three geometric parameter encoding the specific structure of the LFP electrode, i.e. the morpholgy of the battery, viz.

V^i	the individual volumes of the LFP particles ,
A_{E}^i	the individual active surface area of the LFP particles and
A_{AE}	the surface area of the metallic lithium anode .

The particle volume can be determine by an analysis of the electrode composition. Fig. 4 depicts a typical particle size distribution from where the particle volumes can be read off.

The active surface area, more precisely the area where the lithium can intercalate into the iron phosphate lattice cannot be read off from an analysis of the electrode geometry. Coating of the particles as well as the formation of unwanted depositions at particle electrolyte interfaces could be responsible for a decrease of the active surface area. Thus the active surface area is might be smaller as the full particle area. Without further knowledge of the active area we choose for simplicity the full particle surface area corresponding to its volume.

The surface area A_{AE} of the metallic lithium anode is roughly determined by its macroscopic size. But due to the dissolution and deposition of lithium during charging and discharging, the surface is quite rough and A_{AE} might be several orders higher as the macroscopic size. Moreover, in real application the surface area A_{AE} will presumably change and then becomes time dependent. However, this phenomenon is currently not included here.

4 Behavior of the many-particle-electrode model

In this section we show some selected results of numerical simulations of the LFP battery model. We study the influence of (i) charging time, (ii) stochastic noise, (iii) particle size distribution and (iv) active surface areas on the dynamics of the SDE system. Finally we compare our simulations with experimental data.

4.1 Comparison of Fokker-Planck equation and SDE system

A crucial parameter for the simulations is the number of particles N_{P}. Preferable for fast simulations are particle numbers of the order 10^4 whereas in physical reality 10^{17} is a more realistic number. The previously described convergence of the SDE system to the Fokker-Planck system

implies that for N_{P} large enough, the results of the SDE simulations will be stable and close to the solution of the Fokker-Planck system. In order to determine how large N_{P} must be, we compare in this section the simulations via SDE systems with different number of particles and also the simulations of the Fokker-Planck system when available. We select the number N_{P} such that the simulations are stable and close to the Fokker-Planck solution. We assume that such a number N_{P} is the one predicted by the convergence result, and that a simulation with N_{P} is close to the physical reality.

In the case of particles of the same size, simulations are available for both the SDE system and the Fokker-Planck equation [DGH11]. These simulations are in agreement with the convergence of the SDE system to the Fokker-Planck equation. Moreover the simulations show that the (dimensionless) mean chemical potentials for single sized particles obtained from the SDE and the Fokker-Planck equation are related by

$$\langle \mu_{\mathrm{Li}} \rangle(t) \;=\; \tfrac{m_{\mathrm{Li}}}{k_B T} \sum_{i=1}^{N_{\mathrm{P}}} \mu_{\mathrm{Li}}(Y^i(t)) \;\overset{N_{\mathrm{P}}\to\infty}{\longrightarrow}\; \tfrac{m_{\mathrm{Li}}}{k_B T} \int_0^1 \mu_{\mathrm{Li}}(y) p(t,y)\, dy. \tag{34}$$

Then (34) is used to calculate the cell voltage by (18). We observe that the limit (34) is even satisfied for a relatively low number of particles. Figure 3 shows a comparison between the mean chemical potential obtained from the SDE system and from the Fokker-Planck equation for a charging rate of C/20000. Even though in the SDE simulation only 100 particles are used the mean chemical potential according to the SDE system shows qualitatively the same behavior as the mean chemical potential obtained from the Fokker-Planck equation. The SDE simulation shows small fluctuations around the Fokker-Planck simulation due to the stochastic noise term. These fluctuations vanish for an increased number of particles. For more than 3000 particles the fluctuations are not observable anymore.

In the different size case the simulations for the Fokker-Planck system are more difficult and not available at the moment. But the simulations of the mean chemical potential driven by the SDE system are stable for a large number of particles, and actually even for a relatively low number less than 1000 particles. Therefore we assume that simulations with about 5000 particles should be sufficient for the single sized particles and for a particle size distribution as well.

The convergence of the SDE particle system to the Fokker-Planck system, both in the case of single size and different size distribution, will be the topic of a subsequent paper [DFG$^+$16].

4.2 Comparison of single size storage particles and varying storage particle sizes

In this subsection we investigate the microscopic behavior of the system, i.e. the behavior of individual storage particles, as well as the macroscopic behavior, i.e. the battery voltage U, for different charging rates and different particle size distributions.

To study the macroscopic behavior it is convenient to use the (dimensionless) mean chemical

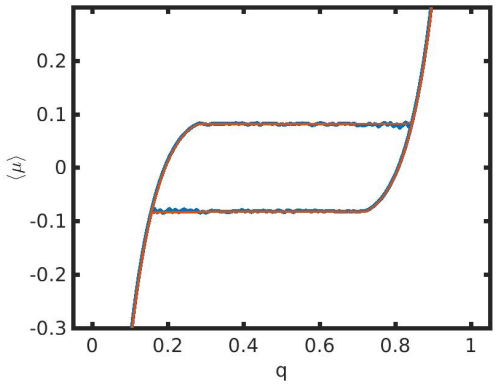

Figure 3: Comparison of Fokker-Planck equation (red) and SDE system with $N_P = 100$ (blue). Full charge-discharge cycle at charging rate 1/20000 C

potential

$$\langle \mu_{\mathrm{Li}} \rangle(t) \;=\; \tfrac{m_{\mathrm{Li}}}{k_B T} \sum_{i=1}^{N_{\mathrm{P}}} \tfrac{A_{\mathrm{E}}^i}{A_{\mathrm{E}}} \mu_{\mathrm{Li}}(Y^i(t)) \;, \tag{35}$$

which is related to the battery voltage U by

$$U = U^{\mathrm{ref}} + \tfrac{m_{\mathrm{Li}}}{e_0}\mu_{\mathrm{Li}}^{\mathrm{ref}} - \tfrac{k_B T}{e_0}\langle \mu_{\mathrm{Li}} \rangle - \tfrac{k_B T}{e_0}\Big(\frac{1}{A_{\mathrm{E}} j_{\mathrm{P}}} + \frac{1}{A_{\mathrm{A}} j_{\mathrm{A}}}\Big) I \;. \tag{36}$$

Thus the characteristic voltage plateaus of LFP electrodes exclusively are a consequence of the mean chemical potential behavior.

Already in the single size case simulations via the Fokker-Planck equation show diverse dynamics sensitively depending on the charging rate and on the stochastic strength [DGH11]. By introducing storage particle size distributions another strong influence on the evolution is added. Here we exclusively study particle size distributions which occur in real life LFP electrodes [SD11, LML$^+$15]. The particle size distribution in Figure 4 serves as a reference distribution. Further distributions are generated by stretching and shifting the reference distribution.

To compare a particle size distribution and a particle system with identical particles we choose the particle size so that the total particle volumes of both systems are equal.

The following simulations are done with approximately 5000 particles.

An analysis of the SDE system shows that a solution $(Y_i^{\text{charge}})_{i=1,\dots,N}$ of a charging process with q_{charge} can be used to define a solution of discharge process by $(Y_i^{\text{discharge}})_{i=1,\dots,N}$ and $q_{\text{discharge}} = 1 - q_{\text{charge}}$ due to the symmetric chemical potential (5). For this reason a simulation of charge and discharge processes with the same charging rate is symmetric. This leads to a symmetric voltage-state of charge plot as it is shown in Figure 3. For this reason we only consider discharge curves. An asymmetry between charging and discharging, which is experimentally observed [SD11], may result from an asymmetric chemical potential μ_{Li}.

Impact of the particle size distribution. In Figure 5 the mean chemical potential $\langle \mu_{\mathrm{Li}} \rangle$ against the state of charge q is plotted for different charging rates. The solution of an ensemble

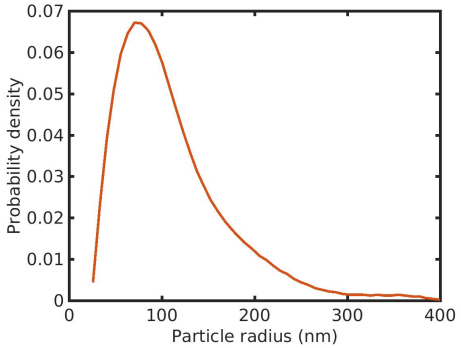

Figure 4: Typical particle size distribution of a LFP electrode.

of identical particles is compared to the solution of the corresponding system with the particle size distribution of Figure 4. In the case of identical particles only the $\langle \mu_{\mathrm{Li}} \rangle$-$q$ plot for the extreme slow charging rate $C/20000$ shows a plateau that corresponds to the observed voltage plateau in LFP batteries, see Figure 1_{right}. However, the other simulations with single sized particles show strong oscillations and a non-monotone behavior. On the other hand all simulation with a particle size distribution exhibit flat plateaus and show bare oscillations. From this observation we conclude that a particle size distribution has a strong impact on the dynamics of the SDE system. Furthermore the simulations show that the SDE system with a particle size distribution predicts the experimental observed voltage plateaus in different charging regimes.

Impact of stochastic fluctuations. In the slow charging regime C/100 the solution of the SDE system for single sized particles depends heavily on the magnitude of the fluctuations, i.e. the choice of the parameter ν_0. Figure 6 shows the influence of the stochastic fluctuations on the mean chemical potential $\langle \mu_{\mathrm{Li}} \rangle$. In the case of the SDE system with identical particle size the differences are severe. Opposed to this there is nearly no observable influence of the fluctuations on the mean chemical potential for the system with a particle size distribution.

For the SDE system with particle size distribution the fluctuations do not produce a relevant effect in the $\langle \mu_{\mathrm{Li}} \rangle$-$q$-plot but it does produce effects at the level of the phase transition.

Phase separation. We start with a simulation with stochastic fluctuations and a charging rate $C/500$. In the single size case, the simulations exhibit a pronounced phase separation, see Figure 7_{left}. Almost all particles are either in the lithium rich phase or in the lithium poor phase. The SDE system with a particle size distribution also shows a pronounced phase separation for a charging rate $C/500$, see Figure 7_{right}. These findings are in agreement with experiments on LFP electrodes [LML$^+$15, LEGF$^+$14, DMC$^+$08].

The simulation with a particle size distribution shows that small particles undergo the phase transition first while larger particles exhibit the phase transition later. However, Figure 7_{right} likewise shows that the phase transition do not exclusively depend on the particle size. There exist a broad region where small and large particles coexist in the same phase. The two-phase region is an effect of the fluctuations and, as we will see, this region vanishes if fluctuations are

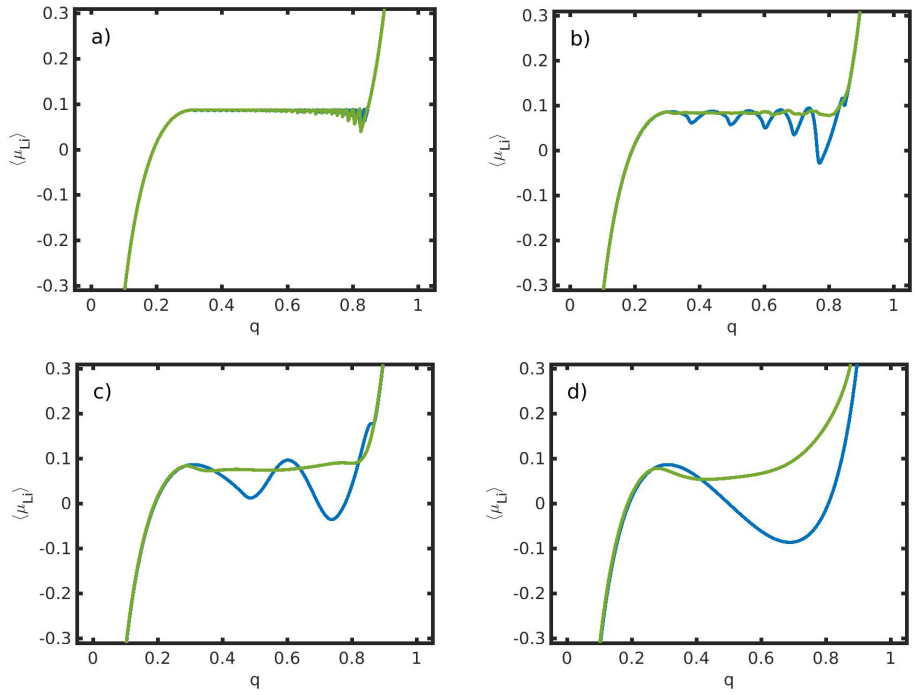

Figure 5: Comparison of simulations with particles of the same size and size distribution. Mean chemical potential $\langle \mu \rangle$ over state of charge q for single size particles (blue) and particle size distribution (green); Charging rate: a) 1/20000 C, b) 1/500 C, c) 1/100 C, d) 1/25 C.

absent, Figure 8_{right}. Furthermore the simulation shows that several large particles remain in an intermediate phase even for a macroscopic time period, i.e. these particles are neither in the lithium rich nor in the lithium poor phase.

In the charging regime C/500 with single size particles, but without stochastic fluctuations, the behavior drastically changes. All particles behave identical and no phase separation is observable anymore, Figure 8_{left}. Conversely, for the SDE system with a particle size distribution a two-phase system is established. Figure 8_{right} shows that the set in of the phase transition is ordered by the particle size.

We consider now the fast charging regime $1C$. In the single size case there is, even under the influence of stochastic noise, no phase separation in the particle system. Figure 9_{left} shows that all particles behave identical. This is in contrast to the slow charging regime where phase separation occurs. In case of a size distribution only small particles reach a lithium rich phase, while the larger particles remain in an intermediate phase, Figure 9_{right}. As before the order of particles undergoing a phase transition depends on the particle size. The same behavior is observed in the slow charging regime.

To summarize, both the particle size distribution and the stochastic fluctuations have a strong impact on the microscopic dynamics of the SDE systems, particularly on the phase separation. In the case of single size particles the simulations without fluctuations or for fast charging do not show phase separation. This is in contrast to experiments on LFP, where phase separa-

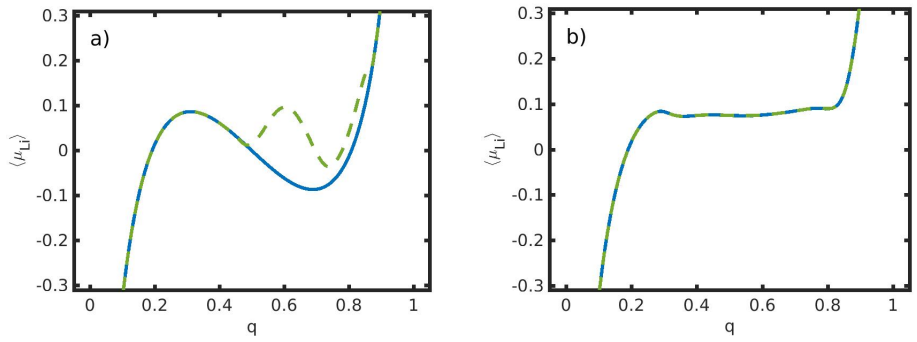

Figure 6: Impact of the stochastic fluctuations on the mean chemical potential $\langle \mu_{\mathrm{Li}} \rangle$. Left: Single size particles without (blue) and with stochastic fluctuations (dashed green), Right: Particle size distribution without (blue) and with stochastic (dashed green). Charging rate 1/100 C.

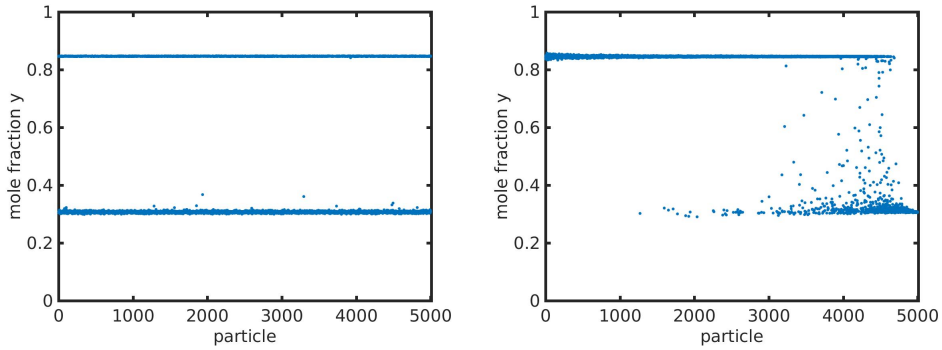

Figure 7: Impact of the particle size distribution on the phase separation at charging rate 1/500 C. Particles are ordered by size. Simulations with stochastic fluctuation. Mole fraction y of the individual storage particles at the state $q = 0.5$. Left: single size particles, Right: particle size distribution.

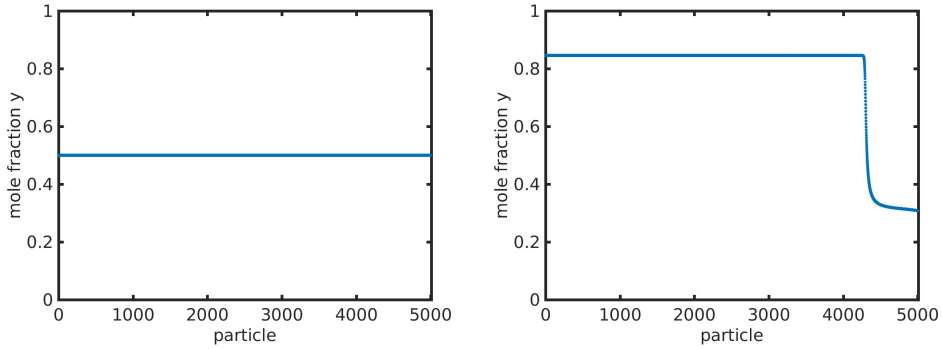

Figure 8: Impact of the particle size distribution on the phase separation at charging rate 1/500 C. Particles ordered by size. Simulations without stochastic fluctuations. Mole fractions y of the individual storage particles at the state $q = 0.5$. Left: single size particles, Right: particle size distribution.

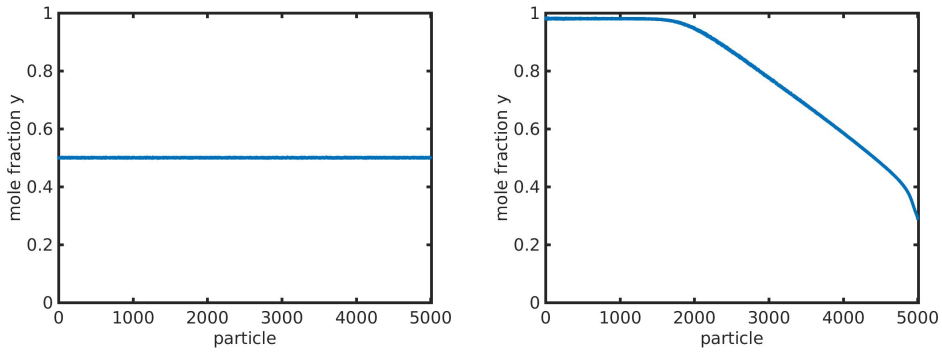

Figure 9: Impact of the particle size distribution on the phase separation at charging rate 1 C. Simulations with stochastic fluctuation. Mole fraction y of the individual storage particle at the state $q = 0.5$. Left: single size particles, Right: particle size distribution (particles ordered by size).

tion is observed. However, all simulations with the particle size distribution from Figure 4 show phase separation within the LFP particle system. The simulations also predict a dependence of the phase transition on the particle size. This finding is experimentally only observed in LFP electrodes where the electric conduction is improved by addition of carbon black [LML$^+$15]. Furthermore the simulations show that larger particles seem to prefer an intermediate state and this behavior is even stronger pronounced for large charging rates. Likewise this finding is in agreement with experiments. Chueh et al. show that in LFP electrodes with small ellipsoidal particles of mean size 230nm two coexisting phases exist whereas electrodes with large platelet particles of mean size 3μm are homogeneous and they are simultaneously filled [LWG$^+$15].

Various particle size distribution. Next we study the effects of different particle size distributions. For simplicity we set the fluctuation strength to zero and we exclusively consider the fast charging regime $1C$. We start with the reference particle size distribution from Figure 4. To generate new size distributions the original distribution ranging from 25nm up to 400nm is now stretched and shifted, respectively. Figure 10 depicts three discharging processes with rate $1C$ for increasingly stretched size distributions. Both the height of the voltage plateau and the value of q, where a sharp drop of the voltage occurs, decrease for increasingly stretched size distributions, i.e. the battery capacity is limited by the charing rate.

In Figure 11 identical size distributions are shifted by a fixed value. Here the voltage decreases as the distribution is shifted to bigger sized particles. However, the rate dependent capacity remains the same if the distribution is shifted.

It is important to recall that particle size distributions with a mean particles size in the micrometer range do not satisfy the assumption of nano-sized LFP particles. However, this assumption is necessary in order to ignore the lithium diffusion within the LFP particles. We expect that diffusion limitation occurs in LFP electrodes if particle sizes above one micrometer are involved. In particlular, for high charging rates diffusion limitation will lead to a further capacity loss. Note that these observations are crucial for a more detailed study on the effects of particle size distributions on the performance of batteries.

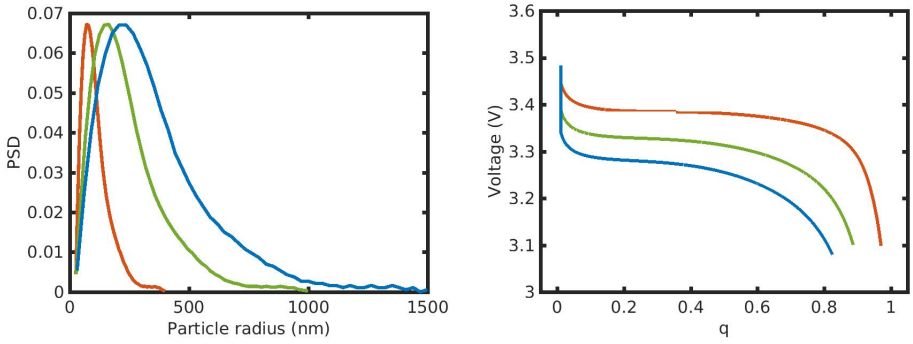

Figure 10: Impact of stretched size distribution: $25-400nm$ (red), $25-1000nm$ (green), $25-1500nm$ (blue); Left: particle size distributions, Right: corresponding voltage for a discharge process at rate $1C$.

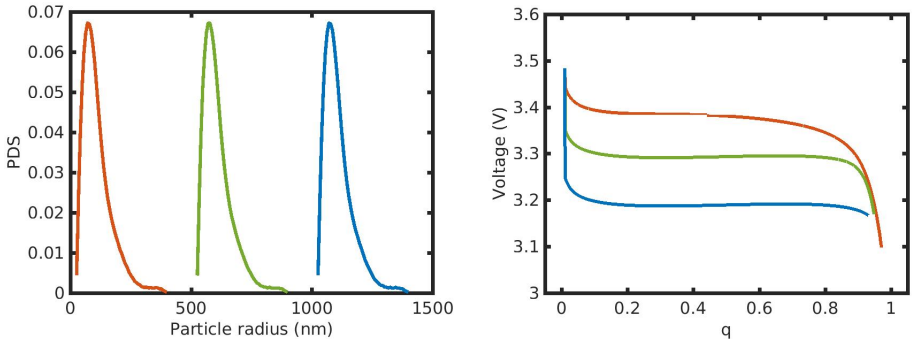

Figure 11: Impact of shifted size distribution: $25-400nm$ (red), $525-900nm$ (green), $1025-1400nm$ (blue); Left: particle size distributions, Right: corresponding voltage for discharge process with rate 1C.

Impact of the active intercalation area. A crucial parameter in our model is the active area A_{E}^{i}, which is the area of particle P^{i} where lithium can intercalate. In batteries this active area depends on the ionic and electronic conductivity of the particle to both the electrode and the electrolyte. Aging processes within the battery such as the formation of solid-electrolyte interfaces may affect the active area. By comparing simulated voltage/capacity plots to experimental data it became clear that a particle size dependent active area shows a more realistic behavior than taking the whole particle area as active. In fact, reducing the active area produces a reduction of the rate depending capacity which is closer to the experimental data. To us it seems reasonable that small particles have a larger ratio of active area to the full particle surface area as large particles. Figure 12_{left} shows three different ratios of active area-particle surface area that are used in the simulations depicted in Figure 12_{right}. The effect of the active area on the battery voltage is shown for a discharge process with rate 1C.

The simulation shows that the active area has a strong impact on the rate depending battery capacity. On the other hand the active area can be positively affected by improving the ionic and electronic conductivity of the particles, for example by surface coating [MDCK^{+}07].

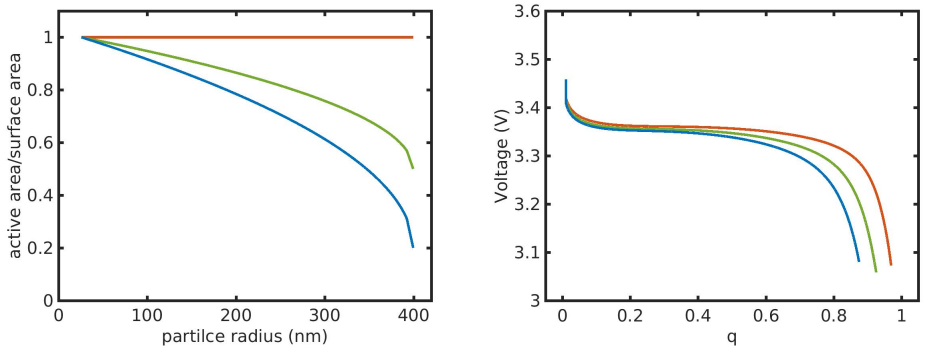

Figure 12: Impact of the active areas: Left: ratio between active area and total area, Right: corresponding voltage for 1C discharge process.

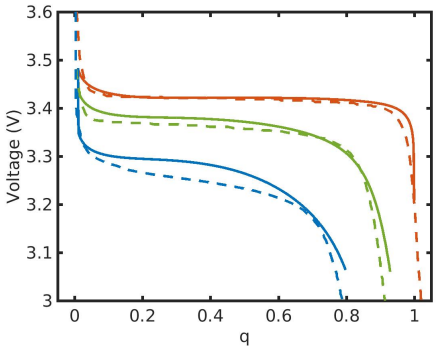

Figure 13: Comparison between simulation and experiment for different charging rates: 1/25 C (red), 1C (green), 3C (blue); Experimental data taken from [SD11]

Impact of the charging rate and fit to the experiments. Figure 13 shows a comparison of experimental data from [SD11] and simulations of the SDE system with the particle size distribution of Figure 4. Three discharging processes with C-rates $C/25$, $1C$ and $3C$ are simulated. The simulations are performed without stochastic fluctuations, since their impact is very limited in moderately fast regime. The active area used for this simulation corresponds to the green curve in Figure 12.

Observe that the maximal possible state of charge q, where the voltage apparently drops, decreases with increasing charging rates. Thus there is a drastic loss of battery capacity for increasing charging rate. Moreover, the height of the voltage plateau decreases for faster rates, i.e. faster charging rates lower the efficiency.

5 Thermodynamic model of a many-particle electrode and its coupling to the surrounding

In this section both the SDE system and the cell voltage- current relation will be derived on a thermodynamic basis. In a first step we describe an electrochemical system in a general ther-

modynamic framework. The model equations are grouped into two different classes: i) universal equations of balance for mass, momentum, energy and entropy and Maxwells equations and ii) constitutive equations that describe the special material properties of the system at hand.

We restrict ourselves to a non-viscous, isothermal, non-polarizable and non-magnetizable systems where accelerations and the magnetic field can be ignored, i.e. the temperature is assumed to be constant, the quasi-static version of the momentum balance and the electrostatic approximation of Maxwells equations is applicable.

Here we present only a brief introduction of the thermodynamic framework, which is absolutely necessary to understand the derivation of the battery model. A detailed description of non-equilibrium thermodynamics and its coupling to electrodynamics can be found in [MR59, dM63, Bed86, Mül85, Guh15].

5.1 General thermodynamic setting

In the general setup we consider an arbitrary domain Ω that is separated by a surface S into two subdomains $\Omega^{\pm}$ so that $S = \partial\Omega^{+} \cap \partial\Omega^{-}$. In order to indicate whether a generic quantity u is defined in the bulk domains $\Omega^{\pm}$ or on the surface S we write $u^{\pm}$ and u_s, respectively.

A point on S is equipped with a surface normal $\boldsymbol{\nu}$ pointing by convention into the domain Ω^{+}.

The boundary ∂S of S is assumed to be a closed line on S that is characterized by a unit vector $\boldsymbol{e}$ lying tangential to S and normal to ∂S.

Constituents and basic quantities. Within the domains $\Omega^{\pm}$ and on the surface S we have general mixtures consisting of $(N^{\pm}+1)$ and (N_s+1) constituents, which are denoted by $A_0, A_1, ..., A_{N^{\pm}}$ and $A_{s,0}, A_{s,1}, ..., A_{s,N_s}$. Each constituent of $\Omega^{\pm}$ is also present on S, but here there may be additional constituents that are exclusively present on S, i.e. $N^{+} + N^{-} \leq N_s$. The set of constituents of the bulk domains and of the surface are denoted by $\mathcal{M}^{\pm}$ and $\mathcal{M}_s$, respectively. Further we assume that the constituents of the bulk domains are different, i.e. $\mathcal{M}^{+} \cap \mathcal{M}^{-} = \emptyset$. In case of identical chemical species in both bulk domains, we treat these species as different constituents. This is reasonable and necessary because a constituent may have different physical and chemical properties in the domains $\Omega^{\pm}$.

The general thermodynamic setting is the same for both domains $\Omega^{\pm}$. Thus for a simplified notation we omit the superscripts $\pm$ and indicate the corresponding domains only if necessary.

The constituent A_0 plays a special role. For example, in an liquid electrolyte A_0 indicates the solvent and in solid electrode A_0 represents the constituent forming the crystal lattice.

In the isothermal and electrostatic setting the thermodynamic state of the bulk mixture is characterized by the number densities $(n_\alpha)_{\alpha\in\mathcal{M}^{\pm}}$, the barycentric velocity $\boldsymbol{v}$ and the electric potential φ. On the surface the thermodynamic state is given by the surface number densities $(n_{s,\alpha})_{\alpha\in\mathcal{M}_s}$, the barycentric surface velocity $\boldsymbol{v}_s$ and the surface electric potential φ_s. These variables may be functions of time and space.

Each constituent A_α of the bulk or surface has the atomic mass m_α and may be carrier of

charge $z_\alpha e_0$, where z_α is the charge number and e_0 is the elementary charge.

Among the surface constituents we may have M_s surface chemical reactions of the general form

$$\mathrm{a}_0^{\mathrm{i}}\mathrm{A}_{\mathrm{s},0} + \cdots + \mathrm{a}_{\mathrm{n_s}}^{\mathrm{i}}\mathrm{A}_{\mathrm{s},\mathrm{N_s}} \underset{R^i_{s,b}}{\overset{R^i_{s,f}}{\rightleftharpoons}} \mathrm{b}_0^{\mathrm{i}}\mathrm{A}_{\mathrm{s},0} + \cdots + \mathrm{b}_{\mathrm{N_s}}^{\mathrm{i}}\mathrm{A}_{\mathrm{s},\mathrm{N_s}} \qquad \text{for i} \in \{1, \cdots, M_s\} \,. \quad (37)$$

The constants a^i_α, b^i_α are positive integers and $\gamma^i_\alpha = b^i_\alpha - a^i_\alpha$ denote the stoichiometric coefficients of the reaction i. $R^i_{s,f}$ and $R^i_{s,b}$ denote the forward and backward reaction rates, respectively. The net reaction rate is defined as $R^i_s = R^i_{s,f} - R^i_{s,b}$.

Multiplication of the number densities n_α by the masses m_α gives the partial mass densities in the bulk and on the surface:

$$\rho_\alpha = m_\alpha n_\alpha \qquad \text{and} \qquad \rho_{s,\alpha} = m_\alpha n_{s,\alpha} \,. \quad (38)$$

For the bulk and surface mixture, the mass densities are defined by

$$\rho = \sum_{\alpha=0}^{N} \rho_\alpha \qquad \text{and} \qquad \rho_s = \sum_{\alpha=0}^{N_s} \rho_{s,\alpha} \,. \quad (39)$$

Finally, the free charge densities are defined by

$$n^{\mathrm{F}} = \sum_{\alpha=0}^{N} z_\alpha e_0 n_\alpha \qquad \text{and} \qquad n^{\mathrm{F}}_s = \sum_{\alpha=0}^{N_s} z_\alpha e_0 n_{s,\alpha} \,. \quad (40)$$

Jumps at the surface. We introduce the boundary values, the jump and the mean value of a generic bulk function $u(t,x) \in \Omega^\pm$ at S as

$$u|^\pm_S = \lim_{x \in \Omega^\pm \to S} u \qquad \text{and} \qquad [\![u]\!] = u|^+_S - u|^-_S \qquad \text{and} \qquad \langle u \rangle = \tfrac{1}{2}(u|^+_S + u|^-_S) \,. \quad (41)$$

In case that the function u is not defined in Ω^+ or in Ω^-, the corresponding value in (41) is set equal to zero.

5.2 Balance of mass and momentum

Customarily non-equilibrium thermodynamics uses the local equations of balance. However, for the derivation of the SDE system it is convenient to use the global version of the mass balances, i.e. in terms of integrals. On the other hand, the momentum balances, Maxwell's equations and the constitutive equations are still represented by their local forms.

Bulk mass balance. The determination of the mass densities $\rho_\alpha = m_\alpha n_\alpha$ relies on the balance equations of mass. The mass of constituent A_α, $\alpha = 0, 1, ..., N$, changes due to convection, diffusion and chemical reactions,

$$\frac{d}{dt}\int_\Omega m_\alpha n_\alpha \, dx = -\int_{\partial\Omega} \boldsymbol{j}_\alpha \cdot \boldsymbol{\nu} \, da + \int_\Omega r_\alpha \, dx \qquad \text{with} \quad \boldsymbol{j}_\alpha = \rho_\alpha(\boldsymbol{v} - \boldsymbol{w}) + \boldsymbol{J}_\alpha \,. \quad (42)$$

The quantities r_α are the mass production densities. Here we do not consider chemical reactions in the bulk domains, i.e. we have $r_\alpha = 0$. The velocity of the boundary $\partial\Omega$ is denoted by $\boldsymbol{w}$ and $\boldsymbol{J}_\alpha$ is the bulk diffusion flux of constituent A_α. To guarantee the total mass conservation the diffusion fluxes satisfy the side condition [MR59, dM63, Mül85]

$$\sum_{\alpha=0}^{N} \boldsymbol{J}_\alpha = 0 \,. \tag{43}$$

Surface mass balance. The surface mass density $\rho_{s,\alpha} = m_\alpha n_{s,\alpha}$, of the surface constituent $A_{s,\alpha}$ is determined by surface mass balance equation,

$$\frac{d}{dt}\int_S m_\alpha n_{s,\alpha}\, da = -\int_{\partial S} \boldsymbol{j}_{s,\alpha}\cdot\boldsymbol{e}\, dl - \int_S [\![\boldsymbol{j}_\alpha\cdot\boldsymbol{\nu}]\!]\, da + \int_S r_{s,\alpha}\, da. \tag{44}$$

The line integral gives the tangential mass flux normal to the line ∂S into the surface S, while the normal flux from the bulk domains across the surface S is represented by the double bracket. The tangential mass flux density is denoted by $\boldsymbol{j}_{s,\alpha}$ and consists of convection and diffusion,

$$\boldsymbol{j}_{s,\alpha} = \rho_{s,\alpha}(\boldsymbol{v}_{\tau,s} - \boldsymbol{w}_\tau) + \boldsymbol{J}_{s,\alpha} \,, \tag{45}$$

where $\boldsymbol{v}_{\tau,s}$ and $\boldsymbol{w}_\tau$ represent the tangential parts of the surface barycentric velocity $\boldsymbol{v}_s$ and of the surface velocity $\boldsymbol{w}$ of S, respectively. The tangential diffusion flux of constituent $A_{s,\alpha}$ on S is denoted by $\boldsymbol{J}_{s,\alpha}$. As in the bulk the diffusion fluxes must satisfy the side condition

$$\sum_{\alpha=0}^{N_s} \boldsymbol{J}_{s,\alpha} = 0 \,. \tag{46}$$

The third term on the right hand side of (44) represents surface chemical reactions with surface mass production densities $r_{s,\alpha}$. The production densities are related to the reaction rates by

$$r_{s,\alpha} = \sum_{i=1}^{M_s} \gamma_{s,\alpha}^i m_\alpha R_s^i \,. \tag{47}$$

Bulk momentum balance. In the quasi-static setting the Cauchy stress $\boldsymbol{\sigma}$ of the matter is balanced by the electrostatic force $-n^{\mathrm{F}}\nabla\varphi$,

$$-\mathrm{div}(\boldsymbol{\sigma}) = -n^{\mathrm{F}}\nabla\varphi \qquad \text{in } \Omega \,. \tag{48}$$

Here the force density due to gravitation is ignored. An alternative formulation of the momentum balance reads, [Mül85, DGM13],

$$\mathrm{div}\boldsymbol{\Sigma} = 0 \qquad \text{in } \Omega \,, \tag{49}$$

where the newly introduced quantity $\boldsymbol{\Sigma}$ is the total stress tensor,

$$\boldsymbol{\Sigma} = \boldsymbol{\sigma} + \varepsilon_0\big(\nabla\varphi\otimes\nabla\varphi - \tfrac{1}{2}|\nabla\varphi|^2\mathbf{1}\big) \,. \tag{50}$$

Surface momentum balance. The quasi-static surface momentum balance equation is represented by, [Mül85, CA65],

$$[\![\boldsymbol{\Sigma} \cdot \nu]\!] = -2k_M \gamma_s \boldsymbol{\nu} - \nabla_s \gamma_s \qquad \text{on } S \,, \tag{51}$$

where γ_s denotes the surface tension and k_M is the mean curvature of the surface S.

5.3 Maxwells equations and electric current

In the quasi-static regime Maxwells equations are significantly reduced. The equations for the electric field $\boldsymbol{E}$ can be solved by introducing an electric potential φ,

$$\boldsymbol{E} = -\nabla\varphi \,. \tag{52}$$

Without polarization the solely relevant Maxwell equation in the bulk is the Poisson equation,

$$\operatorname{div}(\varepsilon_0 \boldsymbol{E}) = n^{\mathrm{F}} \,. \tag{53}$$

The quantity ε_0 is the dielectric constant. Maxwells equations for the surface S separating the bulk domains $\Omega^{\pm}$ are satisfied by (i) a continuous electric potential,

$$\varphi_s = \varphi|_S^+ = \varphi|_S^- \tag{54}$$

and (ii) by the jump condition for the electric field

$$[\![\varepsilon_0 \boldsymbol{E}]\!] \cdot \boldsymbol{\nu} = n_s^{\mathrm{F}} \,. \tag{55}$$

A further crucial equation in electrochemical systems is the electric charge balance,

$$\frac{d}{dt}\int_\Omega n^{\mathrm{e}} dx = -\int_{\partial\Omega} \boldsymbol{j}^{\mathrm{e}} \cdot \boldsymbol{\nu}\, da \quad \text{with} \quad \boldsymbol{j}^{\mathrm{e}} = n^{\mathrm{e}}(\boldsymbol{v} - \boldsymbol{w}) + \boldsymbol{J}^{\mathrm{e}} \,. \tag{56}$$

where n^{e} is the electric charge density and $\boldsymbol{J}^{\mathrm{e}}$ is the electric current density. In a non-polarizable and non-magnetizable system charge density and electric current density are represented by

$$n^{\mathrm{e}} = n^{\mathrm{F}} \qquad \text{and} \qquad \boldsymbol{J}^{\mathrm{e}} = \sum_{\alpha=0}^{N} \tfrac{z_\alpha e_0}{m_\alpha} \boldsymbol{J}_\alpha \,, \tag{57}$$

i.e. they are determined by the number densities and the diffusion fluxes of the constituents. For the surface S the corresponding charge balance reads

$$\frac{d}{dt}\int_S n_s^{\mathrm{e}}\, da = -\int_{\partial S} \boldsymbol{j}_s^{\mathrm{e}} \cdot \boldsymbol{e}\, dl - \int_S [\![\boldsymbol{j}^{\mathrm{e}} \cdot \boldsymbol{\nu}]\!]\, da \qquad \text{with} \qquad \boldsymbol{j}_s^{\mathrm{e}} = n_s^{\mathrm{e}}(\boldsymbol{v}_{\tau,s} - \boldsymbol{w}_\tau) + \boldsymbol{J}_s^{\mathrm{e}} \,. \tag{58}$$

In an analogous manner to the bulk the surface electric charge density n_s^{e} and the surface electric current density $\boldsymbol{J}_s^{\mathrm{e}}$ are given in a non-polarizable and non-magnetizable system by

$$n_s^{\mathrm{e}} = n_s^{\mathrm{F}} \qquad \text{and} \qquad \boldsymbol{J}_s^{\mathrm{e}} = \sum_{\alpha=0}^{N_s} \tfrac{z_\alpha e_0}{m_\alpha} \boldsymbol{J}_{s,\alpha} \,. \tag{59}$$

5.4 Constitutive model

The balance equations for mass and momentum have to be supplemented by constitutive equations for the mass fluxes $\boldsymbol{J}_\alpha$, $\boldsymbol{J}_{s,\alpha}$ and for the surface reaction rates R_s^i. The constitutive equations are restricted by the principle of material objectivity and the 2nd law of thermodynamics consisting of a list of axioms. In the following most results are derived in [dM63, Bed86, BD14, Guh15].

Free energy, chemical potentials and electrochemical potentials. The crucial quantities of a constitutive model are the free energy functions for bulk and surface materials. The free energy functions must be given at first. Then all other constitutive quantities can be represented by the free energy functions and their derivatives in a thermodynamically consistent manner. For the different mixtures of the current study we use free energy functions of the general form

$$\rho\psi = \rho\psi(T, \rho_0, \dots, \rho_N) \qquad \text{and} \qquad \rho_s\psi_s = \rho_s\psi_s(T_s, \rho_{s,0}, \dots, \rho_{s,N_S}) \; . \tag{60}$$

Note that in non-polarizable and non-magnetizable materials, the free energy functions do not explicitly depend on the electromagnetic fields. The interested reader might consult [Mül85, DGM15, Guh15] where more details on polarization and magnetization can be found. In the isothermal setting surface temperature T_s and bulk temperature T are constant and equal in each phase. Therefore the temperature occurs here only as a constant parameter.

The chemical potentials of bulk and surface materials are defined by

$$\mu_\alpha = \frac{\partial\rho\psi}{\partial\rho_\alpha} \qquad \text{and} \qquad \mu_{s,\alpha} = \frac{\partial\rho_s\psi_s}{\partial\rho_{s,\alpha}} \; . \tag{61}$$

In addition to the chemical potentials there are electrochemical potentials which play the central role in the constitutive equations, particularly in the isothermal case. The electrochemical potentials are defined by

$$\mu_\alpha^e = \mu_\alpha + \tfrac{z_\alpha e_0}{m_\alpha}\varphi \qquad \text{and} \qquad \mu_{s,\alpha}^e = \mu_{s,\alpha} + \tfrac{z_\alpha e_0}{m_\alpha}\varphi_s \; . \tag{62}$$

Diffusion fluxes for the bulk domains. The $N+1$ diffusion fluxes $\boldsymbol{J}_\alpha$ must satisfy the side condition (43) so that only N constitutive equations can be given. In the isothermal setting the 2nd law of thermodynamics is guaranteed by the choice [dM63]

$$\boldsymbol{J}_\alpha = -M_\alpha\nabla(\mu_\alpha^e - \mu_0^e) \; , \quad \alpha = 1, \cdots, N \; . \tag{63}$$

The mobility coefficients $M_\alpha > 0$ are non-negative material parameters.

Cauchy stress tensor and pressure. For simplicity, we assume that the viscosity has a minor impact on the battery performance and can be neglected. Then the simplest thermodynamically consistent constitutive equation for the Cauchy stress tensor reads

$$\boldsymbol{\sigma} = -p\mathbf{1} \; , \tag{64}$$

where p is the material pressure satisfying the Gibbs-Duhem equation

$$p = -\rho\psi + \sum_{\alpha=0}^{N} \rho_\alpha \mu_\alpha \, . \tag{65}$$

Diffusion fluxes for the surface S. The equations of surface mass balances (44) have to be supplemented by constitutive equations for the tangential diffusion fluxes $\boldsymbol{J}_{s,\alpha}$ and the normal components of the mass fluxes $\boldsymbol{j}_\alpha$. As in the volume the surface constitutive relations are related to the surface electrochemical potentials. We choose the following thermodynamically consistent constitutive equations for the mass fluxes, [Bed86, Guh15],

$$\boldsymbol{J}_{s,\alpha} = -M_{s,\alpha} \nabla_s (\mu^e_{s,\alpha} - \mu^e_{s,0}) \, , \quad \alpha = 1, \cdots, N_s \, , \tag{66a}$$

$$\boldsymbol{j}_\alpha \cdot \boldsymbol{\nu}|^{\pm}_S = \mp M^{\pm}_{s,\alpha} \big((\mu^e_\alpha - \mu^e_0)|^{\pm}_S - (\mu^e_{s,\alpha} - \mu^e_{s,0}) \big) \, , \quad \alpha = 1, \cdots, N^{\pm} \, , \tag{66b}$$

$$\rho(\boldsymbol{v} - \boldsymbol{w}) \cdot \boldsymbol{\nu}|^{\pm}_S = \mp L^{\pm}_s (\mu^e_0|^{\pm}_S - \mu^e_{s,0} + \pm f) \, , \tag{66c}$$

where $M_{s,\alpha}$, $L^{\pm}_s$ and $M^{\pm}_{s,\alpha}$ denote non-negative material parameter, the so called kinetic coefficients. These constitutive equations embody surface diffusion, (66a), and adsorption from the bulk to the surface S, (66b) and (66c). The newly introduced quantities $f^{\pm}$ will be used to model stochastic processes on the particle surfaces in Section 5.9 .

Note that the surface constitutive equations (66b) and (66c) depend on the constitutive assumptions that were made for the bulks, [Bed86, Guh15]. For example, if we were to consider a viscous material so that viscous term occurs in the constitutive equation for the Cauchy stress (64), then additional viscous terms would likewise arise in the constitutive equation (66c).

Surface tension. The constitutive equation for the surface tension is similar to the Gibbs-Duhem equation for the pressure in the bulk,

$$\gamma_s = \rho_s \psi_s - \sum_{\alpha=0}^{N_s} \rho_{s,\alpha} \mu_{s,\alpha} \, . \tag{67}$$

Surface reaction rates. We use a linear relation between the reaction rate and the corresponding driving force,

$$R^i_s = -R^i_0 \sum_{\alpha=0}^{N_S} \gamma^i_{s,\alpha} m_\alpha \mu^e_{s,\alpha} \, . \tag{68}$$

The kinetic coefficients $R^i_0 > 0$ are called exchange rates.

We refer the reader to [BD14, DGM15, DGM16] where exponential non-linearities of Arrhenius-type were introduced in the constitutive equations for the surface reaction rates so that Butler-Volmer type equations result instead of (68).

5.5 Introduction of stochastic objects in the constitutive model

The constitutive equations for the mass fluxes, reaction rates and stresses have been chosen so that the entropy production becomes a non-negative bilinear form which is zero in equilibrium. In this sense the constitutive equations are compatible with the 2nd law of thermodynamics.

The introduction of the quantities $f^{\pm}$ in the total mass fluxes (66c) is crucial in this work. For this reason we describe here the essential steps for the derivation of the constitutive relations (66b) and (66c).

Let us consider the entropy production ξ_s^ν due to the normal fluxes of momentum, heat and mass across the interface:

$$\begin{aligned}\xi_s^\nu =& \frac{1}{T_s}\Big[\!\Big[\Big(\sigma^{ij} - \Big(\rho\psi - \sum_{\alpha=0}^{N}\rho_\alpha\mu_\alpha\Big)\delta^{ij} - \Big(T_s\rho\big(\tfrac{\mu_0^e}{T} - \tfrac{\mu_{s,0}^e}{T_s}\big)\Big)\delta^{ij}\Big)(v^i - v_s^i)\nu_j\Big]\!\Big] \\ &+ \Big[\!\Big[\Big(q_\nu + \big(T\rho\eta + \sum_{\alpha=0}^{N}\rho_\alpha\mu_\alpha\big)(v_\nu - w_\nu)\Big)\Big(\frac{1}{T} - \frac{1}{T_s}\Big)\Big]\!\Big] \\ &- \Big[\!\Big[\sum_{\alpha=1}^{N} j_{\alpha,\nu}\Big(\tfrac{1}{T}(\mu_\alpha^e - \mu_0^e) - \tfrac{1}{T_s}(\mu_{s,\alpha}^e - \mu_{s,0}^e)\Big)\Big]\!\Big] \,. \end{aligned} \tag{69}$$

A derivation of the entropy production including tangential fluxes and surface reaction can be found in [Bed86] and in the full case of coupled electro- and thermodynamics in [Guh15]. Here q_ν denotes the normal heat flux and $\rho\eta$ is the entropy density of the corresponding bulk domains. The entropy density is related to the free energy by $\rho\eta = -\partial\rho\psi/\partial T$.

The entropy production can be extended by the following observation. The substitution

$$\mu_\alpha^e|_S^{\pm} \;\to\; \mu_\alpha^e|_S^{\pm} + \hat{f}^{\pm} \tag{70}$$

leaves the surface entropy production invariant. Here $\hat{f}^{\pm}$ are arbitrary functions of time and space defined at S that do not depend on the constituent index α.

Next we insert the constitutive equations (64) and (65) for the stress tensor and the pressure, respectively, in (69). Then we choose linear relations for the normal fluxes and obtain the relations

$$\rho(\boldsymbol{v} - \boldsymbol{w})\cdot\boldsymbol{\nu}|_S^{\pm} = \mp L_s^{\pm}T_s(\tfrac{\mu_0^e}{T}|_S^{\pm} - \tfrac{\mu_{s,0}^e}{T_s} + f^{\pm}) \,, \tag{71}$$

$$\Big(q_\nu + \big(T\rho\eta + \sum_{\alpha=0}^{N}\rho_\alpha\mu_\alpha\big)(v_\nu - w_\nu)\Big)|_S^{\pm} = \pm\Big(\kappa_s^{\pm} \mp \big(\rho(v_\nu - w_\nu)f\big)|_S^{\pm}\Big)\Big(\frac{1}{T|_S^{\pm}} - \frac{1}{T_s}\Big) \,, \tag{72}$$

$$\boldsymbol{j}_\alpha\cdot\boldsymbol{\nu}|_S^{\pm} = \mp M_{s,\alpha}^{\pm}T_s\big(\tfrac{1}{T}(\mu_\alpha^e - \mu_0^e)|_S^{\pm} - \frac{1}{T_s}(\mu_{s,\alpha}^e - \mu_{s,0}^e)\big) \,, \tag{73}$$

where we have replaced $\hat{f}$ by f which is defined as $\hat{f} = (\frac{1}{T|_S^{\pm}} - \frac{1}{T_s})f$. Here we are only interested in the isothermal case, thus we set $\kappa_s^{\pm} \to \infty$. Furthermore we assume that $\hat{f}$ is

non-zero in the isothermal case. Thus we have a continuous temperature across the interface,

$$T_s = T|_S^{\pm} \, . \tag{74}$$

Then we obtain the constitutive equations (66b), (66c).

5.6 Special cases of the constitutive model

The constitutive equations for the mass fluxes can be written in the general form

$$F = KD \, , \tag{75}$$

where F represents a mass flux, $K > 0$ is the corresponding kinetic coefficient and D denotes the corresponding thermodynamic driving force.

In this section we consider two important regimes where the kinetic coefficients of the constitutive equations for the mass fluxes assume extreme values, viz.

- $K \to 0$ *slow regime* for diffusion and adsorption ,
- $K \to \infty$ *fast regime* for diffusion and adsorption.

In the slow regime $K \to 0$ the flux is zero and the driving force is independent of the flux. In the fast regime $K \to \infty$ the driving force is zero and the flux is determined by the balance equations. In particular the fast regime leads to some implications, which we study now in more detail.

Infinite bulk mobilities. If the bulk mobility is very large, the fast regime $M_\alpha \to \infty$ is appropriate. For finite diffusion fluxes we must have

$$\nabla(\mu_\alpha^e - \mu_0^e) = 0 \, , \qquad \alpha = 1, 2, ..., N \, . \tag{76}$$

The equations (76) can be further simplified by the condition

$$\sum_{\alpha=0}^{N} m_\alpha n_\alpha \nabla \mu_\alpha^e = 0 \, . \tag{77}$$

This condition follows from a combination of (i) an identity between the spatial gradients of chemical potentials, (ii) the Gibbs-Duhem equation, and (iii) the local form of the quasi-static momentum balance [DGM13].

Inserting (76) into (77) leads to

$$\nabla \mu_\alpha^e = 0 \, , \qquad \alpha = 0, 1, ..., N \, . \tag{78}$$

Thus the electrochemical potentials μ_α^e are the same in every point of the mixture.

Infinite surface mobilities. If the surface mobility is very large, the fast regime $M_{s,\alpha} \to \infty$ is appropriate. In an analogous manner as in the last paragraph we obtain constant surface electrochemical potentials,

$$\nabla_s \, \mu^e_{s,\alpha} = 0 \, , \qquad \alpha = 0, 1, ..., N_s \, . \tag{79}$$

We conclude that the surface electrochemical potentials $\mu^e_{s,\alpha}$ assume the same value in every point of a surface S.

Fast adsorption. The rate of an adsorption process, i.e. the transport of bulk matter to the surface, is determined by the kinetic coefficients $L^{\pm}_s$ and $M^{\pm}_{s,\alpha}$. We talk about fast adsorption of constituent A_0 if $L^{\pm}_s$ assumes a large value. In the fast regime $L^{\pm}_s \to \infty$, we have

$$\mu^e_0|^{\pm}_S - \mu^e_{s,0} + f^{\pm} = 0 \, . \tag{80}$$

Insertion into the constitutive equations (66b) of the other constituents then yields

$$\boldsymbol{j}_\alpha \cdot \boldsymbol{\nu}|^{\pm}_S = \mp M^{\pm}_{s,\alpha}(\mu^e_\alpha|^{\pm}_S - \mu^e_{s,\alpha} + f^{\pm}) \, . \tag{81}$$

If additionally the constituents A_α were also fast adsorbed so that the fast regime $M^{\pm}_{s,\alpha} \to \infty$ is appropriate, the adsorption relation (81) would implying

$$\mu^e_\alpha|^{\pm}_S - \mu^e_{s,\alpha} + f^{\pm} = 0 \, . \tag{82}$$

However the latter case is not considered here.

5.7 Application of the thermodynamic model to the LFP battery

In this section we apply the thermodynamic model to the battery system presented in Figure 1. To this end several assumptions on both the balance equations and the kinetic coefficients are involved to simplify the general thermodynamic model of the last section. The final result will be the LFP battery model introduced in Section 3.

Composition. The LFP battery consists of the many-particle cathode, an electrolyte and a metallic lithium anode as shown in Figure 1 and described in Section 2. For the modeling we decompose the total domain of the battery into volume domains and surface domains.

The N_{P} LFP particles occupy the volume domains Ω^i, $i = 1, 2, ..., N_{\mathrm{P}}$. The volume domains of the metallic substrate of the cathode, the electrolyte and the anode are denoted by Ω_{C}, Ω_{E} and Ω_{A}, respectively.

The total domain is bounded by the upper and lower surfaces S_{U} and S_{L} and by the two electrode surfaces S_{A} and S_{C}. A LFP particle P^i has a common interface with the electrolyte, S^i_{E}, and may have an interface with another particle P^j, which is indicated by S^{ij}. Moreover, the particle P^i may be in contact with the metallic substrate of the cathode via the interface S^i_{C}. Thus the total interface of a particle P^i is given by $S^i = S^i_{\mathrm{C}} \cup S^i_{\mathrm{E}} \cup \sum_j S^{ij}$, where the sum runs

over all particle-particle interfaces of particle P^i. The interface between the metallic substrate of the cathode and the electrolyte, and the interface between the anode and the electrolyte are denoted by $S_{\mathtt{CE}}$ and $S_{\mathtt{AE}}$ respectively.

By convention the normal vector $\boldsymbol{\nu}$ of the surfaces $S^i_{\mathtt{E}}$, $S_{\mathtt{CE}}$, $S_{\mathtt{AE}}$ always points into the electrolyte. The normal vector of the surface $S^i_{\mathtt{C}}$ points into the metal substrate.

Each of the four bulk materials are mixtures with the following constituents: The metal substrate of the cathode and the lithium anode are binary mixtures of metal ions and electrons. We have $(\mathrm{Al}^+, \mathrm{e}^-)$ in the metal substrate of the cathode and $(\mathrm{Li}^+, \mathrm{e}^-)$ in the anode. A LFP particle is formed by the FePO_4 lattice and neutral lithium atoms Li. The constituents of the electrolyte are the lithium cations, Li^+, a solvent S and anions A^-. The constituent A_0 indicates (i) FePO_4 in the LFP particles, (ii) the metal ions Al^+ and Li^+ in cathode and anode, respectively, and (iii) in the electrolyte A_0 represents the solvent.

As assumed in the general setting the constituents of the bulk domains are likewise present on the various interfaces. Moreover, the carbon coating of the LFP particles is a part of the LFP surface. Therefore we have additional surface constituents, viz. (i) C^+ and free electrons e^- on the LFP surfaces.

On the LFP surfaces only one chemical reaction is considered,

$$\mathrm{Li}^+ + \mathrm{e}^- \rightleftharpoons \mathrm{Li} \quad \text{on } S^i \,. \tag{83}$$

Model equations for the LFP particles. The masses of lithium and iron phosphate within a particle P^i changes due to the normal component of the fluxes $\boldsymbol{j}_{\mathrm{Li}}$ and $\boldsymbol{j}_{\mathrm{FePO}_4}$, respectively. The corresponding mass balances (42) read

$$\frac{d}{dt}\int_{\Omega^i} \rho_{\mathrm{Li}}\, dx = -\int_{S^i} \boldsymbol{j}_{\mathrm{Li}} \cdot \boldsymbol{\nu}\, da \,, \qquad \frac{d}{dt}\int_{\Omega^i} \rho_{\mathrm{FePO}_4}\, dx = -\int_{S^i} \boldsymbol{j}_{\mathrm{FePO}_4} \cdot \boldsymbol{\nu}\, da \,. \tag{84}$$

The surface S^i of particle P^i consists of subsurfaces, viz. $S^i = S^i_{\mathtt{C}} \cup S^i_{\mathtt{E}} \cup \sum_j S^{ij}$.

To simplify the mass balances and to specify the lithium flux for the various subsurfaces of the particles we make the following assumptions:

A1 The phase transition within the LFP particles is not observable on the time scale of charging/discharging.

A2 The diffusion of lithium within the LFP particles is fast, i.e. we assume that the fast diffusion regime applies in Ω^i.

A3 There is no lithium exchange between the metal cathode substrate and the particles, i.e. the slow regime for lithium adsorption applies at $S^i_{\mathtt{C}}$.

A4 The contact surface between to particles i and j is small compared to the total particle surface, thus the lithium exchange between to neighboring particles is not significant. The slow regime for lithium adsorption applies on S^{ij}.

A5 The surface constituent $\mathrm{FePO_4}$ is in equilibrium with the bulk constituent $\mathrm{FePO_4}$ of the particles, i.e. we assume that the fast adsorption regime for $\mathrm{FePO_4}$ adsorption applies on the LFP particle surface S^i.

Due to Assumptions A1 and A2 we can apply the reasoning leading to equation (78) of Section 5.6. The chemical potentials within the LFP particles (78) are constant in space, thus

$$\nabla \mu_{\mathrm{Li}} = 0 \qquad \text{and} \qquad \nabla \mu_{\mathrm{FePO_4}} = 0 \quad \text{in } \Omega^i \,. \tag{85}$$

The chemical potentials μ_{Li} and $\mu_{\mathrm{FePO_4}}$ only depend on the number densities of lithium and iron phosphate. We conclude

$$\nabla n_{\mathrm{Li}} = 0 \qquad \text{and} \qquad \nabla n_{\mathrm{FePO_4}} = 0 \quad \text{in } \Omega^i \,. \tag{86}$$

Thus Assumptions A1 and A2 imply that the particles are homogeneous. Note that the value of the number densities depend on the particle index, i.e the number densities assume different values in the particles.

Moreover Assumptions A3 and A4 imply that the normal component of the lithium fluxes are zero at $S^i_{\mathtt{C}}$ and S^{ij}. Thus we have

$$m_{\mathrm{Li}} \frac{d}{dt}(V^i n^i_{\mathrm{Li}}) = -\int_{S^i_{\mathtt{E}}} \boldsymbol{j}_{\mathrm{Li}} \cdot \boldsymbol{\nu} da \qquad \text{and} \qquad m_{\mathrm{FePO_4}} \frac{d}{dt}(V^i n^i_{\mathrm{FePO_4}}) = -\int_{S^i_{\mathtt{E}}} \boldsymbol{j}_{\mathrm{FePO_4}} \cdot \boldsymbol{\nu} da \,. \tag{87}$$

Due to Assumption 4 for $\mathrm{FePO_4}$ we obtain the adsorption relation

$$\mu_{\mathrm{FePO_4}} - \mu_{s,\mathrm{FePO_4}} + f^- = 0 \qquad \text{on } S^i_{\mathtt{E}}. \tag{88}$$

Then the lithium flux on $S^i_{\mathtt{E}}$ is given by

$$\boldsymbol{j}_{\mathrm{Li}} \cdot \boldsymbol{\nu}|^-_{S^i_E} = \tfrac{m_{\mathrm{Li}}}{k_B T} k_{\mathrm{Li}} (\mu_{\mathrm{Li}} - \mu_{s,\mathrm{Li}} + f^-) \qquad \text{on } S^i_{\mathtt{E}} \quad \text{with} \quad k_{\mathrm{Li}} = M^-_{s,\mathrm{Li}} \tfrac{k_B T}{m_{\mathrm{Li}}}. \tag{89}$$

Two remarks: i) Li and $\mathrm{FePO_4}$ have no electric charge, thus in equations (88) and (89) the electrochemical potentials are equal to the chemical potentials. ii) Up to now only the bulk chemical potentials μ_α are constant in space, the surface quantities $\mu_{s,\alpha}$ and f^- may still variate on the particle surface.

Model equations for surfaces of the LFP particles. Next we apply the surface mass balance (44) for lithium to the surface S^i of particle $\mathtt{P}^i$.

For its exploitation we introduce further assumptions:

A6 The tangential transport of the surface constituents $\mathrm{Li}, \mathrm{Li^+}, \mathrm{e^-}, S, A$ is fast, i.e. we apply the fast regime for surface diffusion.

A7 The surface constituents $\mathrm{C^+}$ and $\mathrm{FePO_4}$ move with the particle surfaces, i.e. the tangential fluxes $\boldsymbol{j}_{s,\mathrm{C}}$, $\boldsymbol{j}_{s,\mathrm{FePO_4}}$ are zero.

A8 On S^i the change of masses of all surface constituents are determined by stationary processes.

A9 The chemical reaction $\mathrm{Li}^+ + \mathrm{e}^- \rightleftharpoons \mathrm{Li}$ exclusively occurs on the subsurface $S^i_{\mathtt{E}}$.

A common exploitation of Assumptions A6 and A7 and the reasoning from Section 5.6 imply that the surface electrochemical potentials $\mu^e_{s,\alpha}$ do not depend on the position of the surface S^i,

$$\nabla_s \mu^e_{s,\alpha} = 0, \qquad \text{for } \alpha = \mathrm{Li}, \mathrm{Li}^+, \mathrm{e}^-, \mathrm{C}^+, S, A, \mathrm{FePO}_4 \quad \text{on } S^i_{\mathtt{C}}, S^i_{\mathtt{E}}, S^{ij} \,. \tag{90}$$

The Assumptions A8 and A9 simplify the surface mass balances for surface constituents. For $\alpha = \mathrm{Li}, \mathrm{Li}^+, \mathrm{e}^-, S, A$ we obtain

$$\int_{\partial S} \boldsymbol{j}_{s,\alpha} \cdot \boldsymbol{e}\, dl = -\int_S [\![\boldsymbol{j}_\alpha \cdot \boldsymbol{\nu}]\!]\, da + m_\alpha \gamma_{s,\alpha} \int_S R_s \, da \qquad \text{for} \quad S = S^i_{\mathtt{C}}, S^i_{\mathtt{E}}, S^{ij} \,. \tag{91}$$

These equations are used to determine the corresponding tangential fluxes $\boldsymbol{j}_{s,\alpha}$. The Assumptions A7 and A8 yield that the surface mass balance for C^+ is identically satisfied, and we have for FePO_4

$$\int_S \boldsymbol{j}_{\mathrm{FePO}_4} \cdot \boldsymbol{\nu}\, da = 0 \qquad \text{for} \quad S = S^i_{\mathtt{C}}, S^i_{\mathtt{E}}, S^{ij} \,. \tag{92}$$

Finally due to equation (68) and Assumption A7 the surface reaction rate reads

$$R_s = R^{\mathtt{E}}_0 (m_{\mathrm{Li}^+} \mu^e_{s,\mathrm{Li}^+} + m_{\mathrm{e}^-} \mu^e_{s,\mathrm{e}^-} - m_{\mathrm{Li}} \mu^e_{s,\mathrm{Li}}) \quad \text{on} \quad S^i_{\mathtt{E}} \,. \tag{93}$$

Model equations for the electrolyte. The boundary of the electrolyte domain $\Omega_{\mathtt{E}}$ is given by $S_{\mathtt{E}} = \sum_i S^i_{\mathtt{E}} \cup S_{\mathtt{CE}} \cup S_{\mathtt{AE}} \cup S_{\mathtt{U}} \cup S_{\mathtt{L}}$.

We characterize the electrolyte by the Assumptions

A10 The diffusion of the electrolytic constituents is fast.

A11 The masses of the electrolytic constituents are determined by a stationary process.

A12 There is no adsorption on the surface $S_{\mathtt{CE}}$ of the metallic substrate and on the upper and lower surfaces $S_{\mathtt{U}}$ and $S_{\mathtt{L}}$, respectively. Thus we assume for the electrolytic constituents the slow adsorption regime at $S_{\mathtt{CE}}, S_{\mathtt{U}}, S_{\mathtt{L}}$.

A13 On both the particle-electrolyte surface $S^i_{\mathtt{E}}$ and the anode substrate surface $S_{\mathtt{AE}}$ we have fast adsorption of the solvent and the anions.

A14 The quantity f^+ is set to zero at the anode surface, i.e. we ignore stochastic effects on the anode surface.

According to Section 5.6 the fast diffusion regime, Assumption A10, implies constant electrochemical potentials of the electrolyte species,

$$\nabla \mu_\alpha^e = 0 \qquad \text{for } \alpha = \mathrm{Li}^+, A, S \quad \text{in } \Omega_{\mathtt{E}} \,. \tag{94}$$

In contrast to the LFP particles there are charged constituents in the electrolyte. Thus we cannot replace the electrochemical potentials by the chemical potential. Moreover we cannot conclude that the corresponding number densities are constant.

Assumptions A11 and A12 simplify the bulk mass balance in the electrolyte to

$$0 = \sum_{i=1}^{N_{\mathtt{P}}} \int_{S_{\mathtt{E}}^i} \boldsymbol{j}_\alpha \cdot \boldsymbol{\nu} \, da + \int_{S_{\mathtt{AE}}} \boldsymbol{j}_\alpha \cdot \boldsymbol{\nu} \, da \qquad \alpha = \mathrm{Li}^+, A, S \,. \tag{95}$$

Finally due to Assumption A13 the anions and the solvent must satisfy

$$\mu_\alpha^e - \mu_{s,\alpha}^{\mathrm{e}} + f^+ = 0 \qquad \text{for } \alpha = A, S \qquad \text{on } S_{\mathtt{E}}^i \,, S_{\mathtt{AE}} \,. \tag{96}$$

Then the adsorption fluxes of lithium are represented by

$$\boldsymbol{j}_{\mathrm{Li}^+} \cdot \boldsymbol{\nu}|_{S_E^i}^+ = -M_{s,\mathrm{Li}^+}^{\mathtt{E}} (\mu_{\mathrm{Li}^+}^e - \mu_{s,\mathrm{Li}^+}^e + f^+) \qquad \text{on } S_{\mathtt{E}}^i \,, \tag{97}$$

$$\boldsymbol{j}_{\mathrm{Li}^+} \cdot \boldsymbol{\nu}|_{S_{\mathtt{AE}}}^+ = -M_{s,\mathrm{Li}^+}^{\mathtt{AE}} (\mu_{\mathrm{Li}^+}^e - \mu_{s,\mathrm{Li}^+}^e) \qquad \text{on } S_{\mathtt{AE}} \,. \tag{98}$$

Note that we may have different kinetic coefficients M_{s,Li^+} on $S_{\mathtt{E}}^i$ and $S_{\mathtt{AE}}$. This is indicated by the superscripts. The representation (98) relies on Assumption A14.

Model equations for the electrolyte-anode interface. Both the electrolyte and the metal lithium anode contain lithium ions with the same electric charge number. Even so lithium ions in the liquid electrolyte and the solid lithium anode, respectively, are treated as different constituents in this model because lattice ions have different electrochemical properties as solute ions. At the interface $S_{\mathtt{AE}}$ the different lithium ions are indicated by the subscripts $\mathtt{E}$ and $\mathtt{A}$. The electrolytic lithium ions $\mathrm{Li}_{\mathtt{E}}^+$ can freely move on $S_{\mathtt{AE}}$ whereas the metallic lithium ions of the anode $\mathrm{Li}_{\mathtt{A}}^+$ are fixed in the crystal lattice of the lithium metal. In this context on the anode surface $S_{\mathtt{AE}}$ we have the surface reaction

$$\mathrm{Li}_{\mathtt{E}}^+ \rightleftharpoons \mathrm{Li}_{\mathtt{A}}^+ \qquad \text{on } S_{\mathtt{AE}} \,. \tag{99}$$

The surface $S_{\mathtt{AE}}$ is characterized by the Assumptions

A15 The tangential surface transport of all surface constituents is fast, i.e. the fast regime for surface diffusion is assumed.

A16 On $S_{\mathtt{AE}}$ the masses of all surface constituents are determined by a stationary processes, and there is no tangential mass flux over the boundary $\partial S_{\mathtt{AE}}$.

Assumption A15 implies that the surface electrochemical potentials do not depend on the surface point,

$$\nabla_s \mu^e_{s,\alpha} = 0 \qquad \text{for } \alpha = \mathrm{Li}^+_{\mathtt{A}}, \mathrm{Li}^+_{\mathtt{E}}, \mathrm{e}^-, A, S \quad \text{on } S_{\mathtt{AE}}. \tag{100}$$

Assumption A16 yields for the electrolytic constituents

$$0 = -\int_{S_{\mathtt{AE}}} \boldsymbol{j}_{\mathrm{Li}^+_{\mathtt{E}}} \cdot \boldsymbol{\nu}\, da - m_{\mathrm{Li}^+} \int_{S_{\mathtt{AE}}} R_{s,\mathtt{AE}}\, da \qquad \text{and} \quad 0 = \int_{S_{\mathtt{AE}}} \boldsymbol{j}_\alpha \cdot \boldsymbol{\nu}\, da \qquad \alpha = A, S\,, \tag{101}$$

and for the anode constituents

$$0 = \int_{S_{\mathtt{AE}}} \boldsymbol{j}_{\mathrm{Li}^+_{\mathtt{A}}} \cdot \boldsymbol{\nu}\, da + m_{\mathrm{Li}^+} \int_{S_{\mathtt{AE}}} R_{s,\mathtt{AE}}\, da \qquad \text{and} \qquad 0 = \int_{S_{\mathtt{AE}}} \boldsymbol{j}_{\mathrm{e}^-} \cdot \boldsymbol{\nu}\, da\,. \tag{102}$$

According to (68) the reaction rate $R_{s,\mathtt{AE}}$ reads

$$R_{s,\mathtt{AE}} = R_0^{\mathtt{AE}} m_{\mathrm{Li}^+} (\mu^e_{s,\mathrm{Li}^+_{\mathtt{E}}} - \mu^e_{s,\mathrm{Li}^+_{\mathtt{A}}}) \qquad \text{on } S_{\mathtt{AE}}\,. \tag{103}$$

Model equations for the metal substrate-electrolyte interface. Here we assume

A17 The tangential transport of all surface constituents on $S_{\mathtt{CE}}$ is fast, i.e. we apply the fast regime for surface diffusion.

This Assumption implies that on $S_{\mathtt{CE}}$ the electrochemical potentials are constant in space,

$$\nabla_s \mu^e_{s,\alpha} = 0 \qquad \text{for } \alpha = \mathrm{Al}^+, \mathrm{e}^-, \mathrm{Li}^+, A, S \quad \text{on } S_{\mathtt{CE}}\,. \tag{104}$$

Model equations for the metals. Both the anode and the substrate of the cathode are metals. We assume

A18 The diffusion of the electrons is fast.

A19 There is global charge neutrality in both metals.

A20 On metal surfaces we have fast adsorption of both electrons and metal ions.

Assumption A18 implies in the bulk domains

$$\nabla \mu^e_\alpha = 0 \qquad \alpha = \mathrm{e}^-, \mathrm{Li}^+, \mathrm{Al}^+ \quad \text{in} \quad \Omega_{\mathtt{A}}, \Omega_{\mathtt{C}}\,. \tag{105}$$

We conclude from Assumption A19 that the volume integral under the time derivative of the charge balance (56) vanishes. Thus the charge balance for the anode reads

$$0 = \int_{S_{\mathtt{A}}} \boldsymbol{j}^e \cdot \boldsymbol{\nu}\, da + \int_{S_{\mathtt{AE}}} \boldsymbol{j}^e \cdot \boldsymbol{\nu}\, da\,. \tag{106}$$

The charge balance for the metal substrate of the cathode is represented in a similar manner.

Assumption A20 is now applied to the constitutive equations (66b) and (66c) for adsorption. For the anode it follows

$$\mu_\alpha^e = \mu_{s,\alpha}^e \qquad \alpha = \mathrm{e}^-, \mathrm{Li}^+ \qquad \text{on } S_{\mathtt{AE}}, S_{\mathtt{A}} \,, \tag{107}$$

and for the metal substrate of the cathode we obtain

$$\mu_\alpha^e = \mu_{s,\alpha}^e \qquad \alpha = \mathrm{e}^-, \mathrm{Al}^+ \qquad \text{on } S_{\mathtt{C}}^i, S_{\mathtt{C}}, S_{\mathtt{CE}} \,. \tag{108}$$

Properties of electrochemical potentials at the contact lines. So far our thermodynamic model exclusively treated bulk and surface domains. Additionally we meet contact lines between the different subsurfaces. However, here we will not enter a careful thermodynamic treatment of line phenomena, rather we simply proceed with the Assumption

A21 The electrochemical potentials of electrons, lithium ions and lithium atoms of the two intersecting surfaces are continuous at the corresponding contact line.

This assumption can be derived within thermodynamics of lines if one assumes that the contact line is itself not a carrier of mass, momentum and energy.

The Assumption A21 has far-reaching consequences here: The surface electrochemical potentials of electrons, lithium ions and lithium atoms, respectively, assume the same values on the LFP particle surfaces, i.e. they do not depend on the particle index,

$$\mu_{s,\alpha}^e|_{S^i} = \mu_{s,\alpha}^e \qquad \text{for } \alpha = \mathrm{e}^-, \mathrm{Li}^+, \mathrm{Li} \quad \text{on } S^i \,. \tag{109}$$

Remarks on the momentum balance equation. At first glance the reader may think that until now the momentum balance has not been used. However, this is not the case. Particularly the exploitation of the fast diffusion regime heavily relies on the momentum balance. For example, the momentum balance is needed to conclude that $\nabla(\mu_\alpha^e - \mu_0^e) = 0$ for $\alpha = 1, 2, ..., N$ implies $\nabla \mu_\alpha^e = 0$ for $\alpha = 0, 1, 2, ..., N$, see [DGM13, DGM15] for more details.

Constitutive theory. Until now explicit constitutive equations for the chemical potentials and the pressure were not needed. Moreover an inspection of the model equations reveals that in this study explicit constitutive equations are exclusively needed for the LFP particles. These will be given now. Recall both chemical potentials and pressure are derived from a single free energy function. In [DGG$^+$10, DGH11] a free energy function for LFP is introduced, incorporating (i) the mixing entropy of the distribution of lithium over the interstitial lattices sites of the iron phosphate lattice and (ii) the mechanical deformation of LFP due to the intercalation process. The resulting representations of chemical potentials and the pressure are

$$\mu_{\mathrm{Li}} = \mu_{\mathrm{Li}}^{\mathsf{ref}}(T,p) + \tfrac{1}{m_{\mathrm{Li}}}\Big(L(1-2y) + k_B T\big(\ln(y) - \ln(1-y)\big) \Big) \,, \tag{110}$$

$$\mu_{\mathrm{FePO_4}} = \mu_{\mathrm{FePO_4}}^{\mathsf{ref}}(T,p) + \tfrac{1}{m_{\mathrm{FePO_4}}}\Big(Ly^2 + k_B T \ln(1-y) \Big) \,, \tag{111}$$

$$p = p^{\mathsf{ref}} + K\big((v_{\mathrm{FePO_4}}^{\mathsf{ref}} n_{\mathrm{FePO_4}} + v_{\mathrm{Li}}^{\mathsf{ref}} n_{\mathrm{Li}}) - 1\big) \,. \tag{112}$$

The reference chemical potentials μ_α^{ref} are in general function of temperature and pressure. Here the μ_α^{ref} are calculated by $\mu_{\text{Li}}^{\text{ref}}(T,p) = g_{\text{Li}}(T) + v_{\text{Li}}(p^{\text{ref}} + K\ln(\frac{p-p^{\text{ref}}}{K}+1))$ and $\mu_{\text{FePO}_4}^{\text{ref}}(T,p) = g_{\text{FePO}_4}(T) + v_{\text{FePO}_4}(p^{\text{ref}} + K\ln(\frac{p-p^{\text{ref}}}{K}+1))$. Thus the temperature dependence is left unspecified and the pressure contribution describes linear elastic behavior with volume expansion due to intercalation. The positive constants $v_{\text{FePO}_4}^{\text{ref}}$ and $v_{\text{Li}}^{\text{ref}}$ are the specific volumes of iron phosphate and lithium in LFP. Here p^{ref} is a reference pressure and K is the bulk modulus of LFP. In general the bulk modulus is a function of the lithium content in LFP. For simplicity this is ignored here and K is assumed to be constant.

Volume expansion and surface momentum balance. The intercalation of lithium into the iron phosphate lattice is accompanied by a volume expansion. This is incorporated into the model by the constitutive relation (112). In this study, however, we want to keep the model as simple as possible and neglect the volume expansion. We thus assume

A22 The volume expansion due to intercalation of lithium is negligible, i.e. we set $v_{\text{Li}}^{\text{ref}} = 0$.

It is important to note that the pressure in each particle is still different due to surface tension and mean curvature of the particles. To avoid this complexity a further model simplification becomes necessary. It concerns the surface balance of momentum (51). We assume

A23 The normal component of the total stress $\boldsymbol{\Sigma}$ is continuous at the particle surfaces S^i, i.e.

$$[\![\boldsymbol{\nu}\cdot\boldsymbol{\Sigma}\cdot\boldsymbol{\nu}]\!] = 0 \qquad \text{at } S^i\ . \tag{113}$$

This assumption is satisfied if the product of mean curvature and surface stress is small compared to the total stress.

The outer pressure p_0 acting on the battery surface, i.e. the pressure on $S_{\mathtt{C}}\cup S_{\mathtt{A}}\cup S_{\mathtt{U}}\cup S_{\mathtt{L}}$, is constant. Under the Assumptions A22 and A23 the momentum balance equation yields that the pressure within each particles is given by the outer pressure,

$$p = p_0\ . \tag{114}$$

This implies that the particle density n_{FePO_4} of the iron phosphate lattice of the particles is determined by the constant specific volume,

$$n_{\text{FePO}_4} = (v_{\text{FePO}_4}^{\text{ref}})^{-1} \qquad \text{for all } \Omega^i\ . \tag{115}$$

Moreover we conclude from the mass balance equations (87) and (92) of FePO_4 that the volumes of the LFP particles are time independent,

$$\tfrac{d}{dt}V^i = 0 \qquad \text{for all } i = 1,\dots,N_{\mathtt{P}}\ . \tag{116}$$

Constant number density of iron phosphate and constant pressure within the particles imply that the chemical potentials of lithium only change if the lithium mole fraction $y = n_{\text{Li}}/n_{\text{FePO}_4}$ changes,

$$\mu_{\text{Li}} = \mu_{\text{Li}}(y)\ . \tag{117}$$

5.8 Evolution equations for the lithium mole fractions of the LFP battery model

The balance equation (87) and the corresponding constitutive equation for the mass flux (89) form the basis of the LFP battery model.

Due to the assumptions of the last subsection, the lithium mass flux normal to the surface S_{E}^i is spatially constant if we assume a spatially constant f^- on S_{E}^i,

$$\boldsymbol{j}_{\mathrm{Li}} \cdot \boldsymbol{\nu}|_{S_{\mathrm{E}}^i}^- = \tfrac{m_{\mathrm{Li}}}{k_B T} k_{\mathrm{Li}} \Big(\mu_{\mathrm{Li}}(y^i) - \mu_{s,\mathrm{Li}} + f^{i,-} \Big) \qquad \text{at } S_{\mathrm{E}}^i \,. \tag{118}$$

Finally we use (115),(116) and (118) so that the lithium mass balance equations (89) becomes the central evolution equation of this study: For $i = 1, \ldots, N_{\mathrm{P}}$

$$\frac{dy^i}{dt} = \frac{1}{\tau^i} \frac{m_{\mathrm{Li}}}{k_B T} \big(\mu_{s,\mathrm{Li}} - \mu_{\mathrm{Li}}(y^i) - f^{i,-} \big) \quad \text{with} \quad \frac{1}{\tau^i} = \frac{k_{\mathrm{Li}}}{m_{\mathrm{Li}} n_{\mathrm{FePO_4}}} \frac{A_{\mathrm{E}}^i}{V^i} \,. \tag{119}$$

5.9 Wiener process

In this section we will use the objects $(f^i)_{(i=1,\ldots,N_{\mathrm{P}})}$ to represent some stochastic phenomena within the LFP model. Note that in Section 5.5 the f^i are introduced in a thermodynamically consistent manner as free objects in the constitutive theory. For the following discussion we write the evolution equations (119) in the generic form

$$\frac{dy^i}{dt} = a^i(t, y^1, .., y^{N_{\mathrm{P}}}) + b^i(t, y^1, .., y^{N_{\mathrm{P}}}) \xi^i(t). \tag{120}$$

Assuming that the quantities a^i and b^i are classical functions and ξ^i are stochastic forces representing *white noise*, then the equations (120) are called Langevin equations. Roughly speaking $\xi^i(t)$ is called white noise if its time mean is zero and if the time mean of $(\xi^i(t)\xi^j(t'))$ is given by a Dirac distribution, $\delta(t-t')\delta^{ij}$. In other words, the values of $\xi^i(t)$ at different times and for different i, j are not correlated. However, in the next two paragraphs we will sketch that for white noise the derivatives $\frac{dy^i}{dt}$ do not exist. For this reason it is only possible to consider (120) in the integral form

$$y^i(t) - y^i(t_0) = \int_{t_0}^{t} a^i(s, y^1(s), .., y^{N_{\mathrm{P}}}(s)) ds + \int_{t_0}^{t} b^i(s, y^1(s), .., y^{N_{\mathrm{P}}}(s)) \xi^i(s) ds. \tag{121}$$

Moreover, the second integral cannot be considered as a Riemann integral, because the Riemann integral over white noise, for example $\int_0^t \xi(s) ds$, does not exist but must be newly interpreted as an Ito integral, see [Gar96] for more details.

Definition of the Wiener process. For $t \geq 0$ we consider the vector-valued stochastic process

$$\boldsymbol{Y}(t) = (Y^1(t), ..., Y^{N_{\mathrm{P}}}(t)) \quad \text{with values} \quad \boldsymbol{y}(t) = (y^1(t), ..., y^{N_{\mathrm{P}}}(t)) \,. \tag{122}$$

We are interested in a stochastic process that is a special case of a Markov process: the Wiener process.

In this paper we characterize the Wiener process by the conditional probability density $p(\boldsymbol{y}, t|\boldsymbol{y_0}, t_0) \geq 0$. The quantity $p(\boldsymbol{y}, t|\boldsymbol{y_0}, t_0)d\boldsymbol{y}$ determines the probability that the stochastic variable $\boldsymbol{Y}$ assuming the value $\boldsymbol{y_0}$ at time $t_0 \leq t$ is at time t in the interval $\boldsymbol{y} + d\boldsymbol{y}$. A stochastic process $\boldsymbol{Y}(t)$ is called Wiener process if the possible values of the process are distributed according to the probability density

$$p(\boldsymbol{y}, t|\boldsymbol{y_0}, t_0) = \frac{1}{\sqrt{2\pi(t-t_0)}^{N_\mathrm{P}}} \exp\left(-\frac{(\boldsymbol{y}-\boldsymbol{y}_0)^2}{2(t-t_0)}\right). \tag{123}$$

The probability density is normalized,

$$\int_{-\infty}^{\infty} p(\boldsymbol{y}, t|\boldsymbol{y_0}, t_0)d\boldsymbol{y} = 1, \tag{124}$$

and mean value and variance, respectively, are given by

$$\int_{-\infty}^{\infty} \boldsymbol{y}\, p(\boldsymbol{y}, t|\boldsymbol{y_0}, t_0)d\boldsymbol{y} = \boldsymbol{y}_0, \quad \int_{-\infty}^{\infty} (y^i - y^i)(y^j - y^j)\, p(\boldsymbol{y}, t|\boldsymbol{y_0}, t_0)d\boldsymbol{y} = (t-t_0)\delta_{ij}. \tag{125}$$

Some properties of the Wiener process. We follow Gardiner, [Gar96], to show that a Wiener process, $W(t)$ with values $w(t)$, is continuous but not differentiable. Obviously we deduce from (123):

$$\lim_{h\to 0} p(\boldsymbol{w}, t+h|\boldsymbol{w_0}, t)\frac{1}{h} = 0 \quad \text{uniformly in} \quad \boldsymbol{w},\ \boldsymbol{w}_0,\ t \tag{126}$$

for $|\boldsymbol{y} - \boldsymbol{y}_0| \geq \varepsilon > 0$. Next we calculate the probability of the inequality $|\boldsymbol{W}(t+h) - \boldsymbol{W}(t)|/h > C$ with $h, C > 0$. Particularly we are interested in the limit $h \to 0$ for arbitrary chosen positive C. In other words, we ask for the differentiability of the Wiener process. To this end it suffices to consider a single stochastic variable. We calculate

$$\begin{aligned}
\text{prob}\{|\frac{W(t+h)-W(t)}{h}| > C\} &= \int_{-\infty}^{-hC} p(w, t+h|0, t)dy + \int_{hC}^{\infty} p(w, t+h|0, t)dw \\
&= 2\int_{hC}^{\infty} p(w, t+h|0, t) = \frac{2}{\sqrt{2\pi h}}\int_{hC}^{\infty} \exp\left(-\frac{w^2}{2h}\right)dw \\
&= \frac{2}{\sqrt{\pi}}\int_{C\sqrt{\frac{h}{2}}}^{\infty} \exp\left(-w^2\right)dw \overset{h\to 0}{\to} 1\,.
\end{aligned} \tag{127}$$

Thus at any time the derivative of the Wiener process is arbitrary large with probability one.

White noise and Wiener process. In [Gar96] it is shown that the Riemann integral $\int_0^t \xi(s)ds$ is equal to $W(t)$. However, the last paragraph reveals that $\dot{W}$ does not exist. Thus in our context we need a new interpretation and new rules for the integral $\int_{t_0}^t b^i(s, y^1, .., y^{N_\mathrm{P}})\xi^i(s)ds$. We write $\int_{t_0}^t b^i(s, y^1, .., y^{N_\mathrm{P}})dW^i$ and interpret this integral as an Ito integral with a new calculus, Ito-calculus, that must be used for exploitation, see again Gardiner [Gar96].

In our case the functions b^i are given by constants, viz. $b^i = \nu^i\sqrt{2/\tau^i}$, so we have

$$\int_{t_0}^{t} b^i(s, y^1, .., y^{N_\mathrm{P}})\xi^i(s)ds = \nu^i\sqrt{\frac{2}{\tau^i}}(W^i(t) - W^i(t_0)). \tag{128}$$

5.10 Charge transport

The charge is transported by the lithium ions from the anode to the cathode, whereby the electrons have to flow through an electric device. The electric device is connected to the battery via the surfaces $S_\mathtt{A}$ and $S_\mathtt{C}$.

We define the electric current I of the battery by the electric current density $\boldsymbol{j}^e$ which flows through the outer anode surface $S_\mathtt{A}$., viz.

$$I = \int_{S_\mathtt{A}} \boldsymbol{j}^\mathrm{e} \cdot \boldsymbol{\nu}\, da \qquad \text{with} \quad \boldsymbol{j}^\mathrm{e} = \sum_{\alpha=\mathrm{e}^-,\mathrm{Li}^+} \frac{e_0 z_\alpha}{m_\alpha}\boldsymbol{j}_\alpha\ . \tag{129}$$

Using the mass balances (106), (101), (102), (95) and (91) we conclude

$$I = \frac{e_0}{m_{\mathrm{Li}^+}}\int_{S_\mathtt{AE}} \boldsymbol{j}_{\mathrm{Li}^+}\cdot\boldsymbol{\nu}\, da = -\frac{e_0}{m_{\mathrm{Li}^+}}\sum_{i=1}^{N_\mathrm{P}}\int_{S_\mathtt{E}^i} \boldsymbol{j}_{\mathrm{Li}^+}\cdot\boldsymbol{\nu}\, da = -\frac{e_0}{m_{\mathrm{Li}}}\sum_{i=1}^{N_\mathrm{P}}\int_{S_\mathtt{E}^i} \boldsymbol{j}_{\mathrm{Li}}\cdot\boldsymbol{\nu}\, da\ . \tag{130}$$

In a further step we replace the lithium fluxes of the electrolyte side by the fluxes of stored lithium in the LFP particles. To this end we use equation (87) and then obtain a relation between the current and the total lithium mole fraction that we seek for,

$$I \quad = e_0 n_{\mathrm{FePO_4}} V_\mathtt{P}\frac{d}{dt}\Big(\sum_{i=1}^{N_\mathrm{P}}\frac{V^i}{V_\mathtt{P}}y^i\Big) \quad = e_0 n_{\mathrm{FePO_4}} V_\mathtt{P}\frac{dq}{dt}\ . \tag{131}$$

This equation expresses the intuitive relation that the electric current is directly related to the amount of stored lithium in the ensemble of LFP particles.

A further important observation is that the relation (131) is exclusively derived from balance equations. Thus the equation (131) is independent of the constitutive equations and especially of the materials at hand. Note, we have assumed that the mass balances at the surfaces, in both metals and electrolyte are stationary. This implies that the electric charge is exclusively stored in the LFP particles. In particular without the stationary balance equations for the LFP particles, a surface contribution would appear in (131).

5.11 Battery voltage

The electric potential difference between the metallic substrate of the cathode at the surface $S_{\mathtt{C}}$ and of the anode at $S_{\mathtt{A}}$ defines the cell voltage

$$U = \varphi|_{S_{\mathtt{C}}} - \varphi|_{S_{\mathtt{A}}} \,. \tag{132}$$

Herein we use the electrochemical potentials, $\mu^e_\alpha = \mu_\alpha + \frac{e_0 z_\alpha}{m_\alpha}\,\varphi$, for the electrons in the substrate of the cathode and for lithium ions in the anode to obtain

$$U = \tfrac{m_{\mathrm{e}^-}}{e_0}(\mu_{\mathrm{e}^-} - \mu^e_{\mathrm{e}^-})|_{S_{\mathtt{C}}} + \tfrac{m_{\mathrm{Li}^+}}{e_0}(\mu_{\mathrm{Li}^+_{\mathtt{A}}} - \mu^e_{\mathrm{Li}^+_{\mathtt{A}}})|_{S_{\mathtt{A}}} \,. \tag{133}$$

The assumptions of fast diffusion and fast adsorption for the electrons in the cathode imply that its electrochemical potential $\mu^e_{e^-}$ is the same everywhere in the cathode where electrons exist. In particular we have $\mu^e_{s,\mathrm{e}^-}|_{S_{\mathtt{E}}} = \mu^e_{\mathrm{e}^-}|_{S_{\mathtt{C}}}$, where $S_{\mathtt{E}}$ is an abbreviation for $S_{\mathtt{E}} = \cup_i S^i_{\mathtt{E}}$. The fast diffusion assumption for the anode implies that the electrochemical potential of the lithium ions in the anode is everywhere the same and thus we have $\mu^e_{s,\mathrm{Li}^+_{\mathtt{A}}}|_{S_{\mathtt{AE}}} = \mu^e_{\mathrm{Li}^+_{\mathtt{A}}}|_{S_{\mathtt{A}}}$.

Thus we may write

$$U = \tfrac{m_{\mathrm{e}^-}}{e_0}\big(\mu_{\mathrm{e}^-}|_{S_{\mathtt{C}}} - \mu^e_{s,\mathrm{e}^-}|_{S_{\mathtt{E}}}\big) + \tfrac{m_{\mathrm{Li}^+}}{e_0}\big(\mu_{\mathrm{Li}^+_{\mathtt{A}}}|_{S_{\mathtt{A}}} - \mu^e_{s,\mathrm{Li}^+_{\mathtt{A}}}|_{S_{\mathtt{AE}}}\big) \,. \tag{134}$$

In order to generate differences that can be represented by adsorption fluxes and the reaction rate, respectively, we add some new terms that cancel each other,

$$\begin{aligned}
U =& \tfrac{1}{e_0}\big(m_{\mathrm{Li}^+}\mu_{\mathrm{Li}^+_{\mathtt{A}}}|_{S_{\mathtt{A}}} + m_{\mathrm{e}^-}\mu_{\mathrm{e}^-}|_{S_{\mathtt{C}}}\big) \\
&- \tfrac{1}{e_0}\big(m_{\mathrm{Li}^+}\mu^e_{s,\mathrm{Li}^+_{\mathtt{A}}}|_{S_{\mathtt{AE}}} - m_{\mathrm{Li}^+}\mu^e_{s,\mathrm{Li}^+}|_{S_{\mathtt{AE}}}\big) \\
&- \tfrac{1}{e_0}\big(m_{\mathrm{Li}^+}\mu^e_{s,\mathrm{Li}^+}|_{S_{\mathtt{AE}}} - m_{\mathrm{Li}^+}\mu^e_{\mathrm{Li}^+}|^+_{S_{\mathtt{AE}}}\big) \\
&- \tfrac{1}{e_0}\big(m_{\mathrm{Li}^+}\mu^e_{\mathrm{Li}^+}|^+_{S_{\mathtt{AE}}} - m_{\mathrm{Li}^+}\mu^e_{\mathrm{Li}^+}|^+_{S_{\mathtt{E}}}\big) \\
&- \tfrac{1}{e_0}\big(m_{\mathrm{Li}^+}\mu^e_{\mathrm{Li}^+}|^+_{S_{\mathtt{E}}} - m_{\mathrm{Li}^+}\mu^e_{s,\mathrm{Li}^+}|_{S_{\mathtt{E}}}\big) \\
&- \tfrac{1}{e_0}\big(m_{\mathrm{Li}^+}\mu^e_{s,\mathrm{Li}^+}|_{S_{\mathtt{E}}} + m_{\mathrm{e}^-}\mu^e_{s,\mathrm{e}^-}|_{S_{\mathtt{E}}} - m_{\mathrm{Li}}\mu^e_{s,\mathrm{Li}}|_{S_{\mathtt{E}}}\big) \\
&- \tfrac{m_{\mathrm{Li}}}{e_0}\sum_{i=1}^{N_{\mathtt{P}}}\frac{A^i_{\mathtt{E}}}{A_{\mathtt{E}}}(\mu^e_{s,\mathrm{Li}} - \mu^e_{\mathrm{Li}})|_{S^i_{\mathtt{E}}} - \tfrac{m_{\mathrm{Li}}}{e_0}\sum_{i=1}^{N_{\mathtt{P}}}\frac{A^i_{\mathtt{E}}}{A_{\mathtt{E}}}\mu^e_{\mathrm{Li}}|_{S^i_{\mathtt{E}}} \,.
\end{aligned} \tag{135}$$

Next we use the relations (103),(98),(94),(97),(93), (89) and (117) to replace in (135) the chem-

ical potential differences,

$$
\begin{aligned}
U =& \tfrac{1}{e_0}\big(m_{\mathrm{Li^+}}\mu_{\mathrm{Li^+_A}}|_{S_{\mathtt{A}}} + m_{\mathrm{e^-}}\mu_{\mathrm{e^-}}|_{S_{\mathtt{C}}}\big) \\
& \tfrac{1}{e_0 R_0^{\mathtt{AE}}} R_{s,\mathtt{AE}} \\
& - \frac{m_{\mathrm{Li^+}}}{e_0 M^{\mathtt{AE}}_{s,\mathrm{Li^+}}} \frac{1}{A_{\mathtt{AE}}} \int_{S_{\mathtt{AE}}} \boldsymbol{j}_{\mathrm{Li^+}} \cdot \boldsymbol{\nu}\, da \\
& + \frac{m_{\mathrm{Li^+}}}{e_0 M^{\mathtt{E}}_{s,\mathrm{Li^+}}} \sum_{i=1}^{N_{\mathtt{P}}} \frac{A^i_{\mathtt{E}}}{A_{\mathtt{E}}} (\boldsymbol{j}_{\mathrm{Li^+}} \cdot \boldsymbol{\nu})|_{S^i_{\mathtt{E}}} + \frac{m_{\mathrm{Li}}}{e_0} \sum_{i=1}^{N_{\mathtt{P}}} \frac{A^i_{\mathtt{E}}}{A_{\mathtt{E}}} f^+|_{S^i_{\mathtt{E}}} \\
& - \tfrac{1}{e_0 R_0^{\mathtt{E}}} R_s \\
& + \tfrac{k_B T}{e_0} \tfrac{1}{k_{\mathrm{Li}}} \sum_{i=1}^{N_{\mathtt{P}}} \frac{A^i_{\mathtt{E}}}{A_{\mathtt{E}}} \boldsymbol{j}_{\mathrm{Li}} \cdot \boldsymbol{\nu}|_{S^i_{\mathtt{E}}} - \tfrac{m_{\mathrm{Li}}}{e_0} \sum_{i=1}^{N_{\mathtt{P}}} \tfrac{A^i_{\mathtt{E}}}{A_{\mathtt{E}}} f^-|_{S^i_{\mathtt{E}}} - \tfrac{m_{\mathrm{Li}}}{e_0} \sum_{i=1}^{N_{\mathtt{P}}} \tfrac{A^i_{\mathtt{E}}}{A_{\mathtt{E}}} \mu_{\mathrm{Li}}(y^i)\,. \qquad (136)
\end{aligned}
$$

Note that a choice of the function f^+ has not been made up to now. Therefore we can use $f^+ = f^-$ to eliminate f^- in (136). In the next step we replace the mass fluxes and the reaction rate by the current I. To this end we use the equations (101), (130) and (91) and obtain

$$
\begin{aligned}
U =& \tfrac{1}{e_0}\big(m_{\mathrm{Li^+}}\mu_{\mathrm{Li^+_A}}|_{S_{\mathtt{A}}} + m_{\mathrm{e^-}}\mu_{\mathrm{e^-}}|_{S_{\mathtt{C}}}\big) \\
& - \Big(\tfrac{1}{e_0^2 R_0^{\mathtt{AE}}} \tfrac{1}{A_{\mathtt{AE}}} + \tfrac{(m_{\mathrm{Li^+}})^2}{e_0^2 M^{\mathtt{AE}}_{s,\mathrm{Li^+}}} \tfrac{1}{A_{\mathtt{AE}}} + \tfrac{(m_{\mathrm{Li^+}})^2}{e_0^2 M^{\mathtt{E}}_{s,\mathrm{Li^+}}} \tfrac{1}{A_{\mathtt{E}}} + \tfrac{1}{e_0^2 R_0^{\mathtt{E}}} \tfrac{1}{A_{\mathtt{E}}} + \tfrac{m_{\mathrm{Li}} k_B T}{e_0^2} \tfrac{1}{k_{\mathrm{Li}}} \tfrac{1}{A_{\mathtt{E}}}\Big) I \\
& - \tfrac{m_{\mathrm{Li}}}{e_0} \sum_{i=1}^{N_{\mathtt{P}}} \frac{A^i_{\mathtt{E}}}{A_{\mathtt{E}}} \mu_{\mathrm{Li}}(y^i)\,. \qquad (137)
\end{aligned}
$$

Finally we introduce the abbreviations

$$
U^{\mathrm{ref}} = \tfrac{1}{e_0}\big(m_{\mathrm{Li^+}}\mu_{\mathrm{Li^+_A}}|_{S_{\mathtt{A}}} + m_{\mathrm{e^-}}\mu_{\mathrm{e^-}}|_{S_{\mathtt{C}}} - m_{\mathrm{Li}}\mu^{\mathrm{ref}}_{\mathrm{Li}}\big) \qquad (138)
$$

and

$$
\begin{aligned}
& j^{\mathtt{P}}_{\mathrm{ic}} = \tfrac{e_0}{m_{\mathrm{Li}}} k_{\mathrm{Li}}\,, && j^{\mathtt{P}}_{\mathrm{ad}} = \frac{e_0 k_B T M^{\mathtt{E}}_{s,\mathrm{Li^+}}}{(m_{\mathrm{Li^+}})^2}\,, && j^{\mathtt{P}}_{\mathrm{re}} = e_0 k_B T R_0^{\mathtt{E}}\,, \\
& j^{\mathtt{A}}_{\mathrm{de}} = e_0 k_B T R_0^{\mathtt{AE}}\,, && j^{\mathtt{A}}_{\mathrm{ad}} = \frac{e_0 k_B T M^{\mathtt{AE}}_{s,\mathrm{Li^+}}}{(m_{\mathrm{Li^+}})^2}\,. && \qquad (139)
\end{aligned}
$$

Then we obtain a relation that relates the thermodynamic state of the battery to the battery voltage,

$$
U = U^{\mathrm{ref}} - \tfrac{m_{\mathrm{Li}}}{e_0} \sum_{i=1}^{N_{\mathtt{P}}} \tfrac{A^i_{\mathtt{E}}}{A_{\mathtt{E}}} \big(\mu_{\mathrm{Li}}(y^i) - \mu^{\mathrm{ref}}_{\mathrm{Li}}\big) - \tfrac{k_B T}{e_0} \tfrac{1}{A_{\mathtt{E}}} \Big(\tfrac{1}{j^{\mathtt{P}}_{\mathrm{ad}}} + \tfrac{1}{j^{\mathtt{P}}_{\mathrm{re}}} + \tfrac{1}{j^{\mathtt{P}}_{\mathrm{ic}}}\Big) I - \tfrac{k_B T}{e_0} \tfrac{1}{A_{\mathtt{AE}}} \Big(\tfrac{1}{j^{\mathtt{A}}_{\mathrm{de}}} + \tfrac{1}{j^{\mathtt{A}}_{\mathrm{ad}}}\Big) I\,. \qquad (140)
$$

6 Discussion and outlook

The numerical investigations of this paper demonstrate the adequate representation of the LFP battery by our stochastic battery model. The model embodies both the phase transition and the

battery voltage for varying charging speeds. Special emphasis is placed to predict the influence of the particle size distribution on the battery voltage.

The dynamics of the model are determined by the size distribution of storage particles and furthermore by only two constant kinetic parameter, viz. the intercalation rate k_{Li} and the strength of the fluctuations, ν_0. These parameter play quite different roles in the model. The simulations reveal that the intercalation rate determines the macroscopic behavior of the electrode, i.e. the battery voltage as a function of the state of charge of the battery. The derived voltage-current relation (18) likewise shows that intercalation is the dominant phenomena to predict the discharging-charging process.

On the other hand the strength of fluctuations on the particle surfaces characterizes the inset of the phase transition which is additionally influenced by the size distribution of the particles. However, the size distribution effect is weaker pronounced in the experiment, [LML$^+$15], compared to the model. Certainly this difference between experiment and model is induced by our assumption of fast tangential charge transport on the particle surfaces, see Assumption 10 on page 34. If the surface charge transport was limited by a finite surface mobility, the phase transition would be more affected by the coupling of the LFP electrode to the electrolyte than by the size distribution of the particles.

A further model assumption states that charge transport within the electrolyte is fast with respect to the surface processes. Then the general constitutive equations imply constant electrochemical potentials in the electrolyte. For known geometry of the electrodes we could use the Poisson equation and the constant electrochemical potentials to determine the electric potential and the distribution of ions in the electrolyte. In particular, by means of suitable electrolyte models [DGM13, DGM15] the dimension of the electric double layer within the pore space of the LFP electrode could be studied. Then it could be tested if the assumption of electroneutrality in the electrolyte, which is met in many other battery models, is appropriate.

The stochastic model of this paper is not restricted to a LFP electrode against a metallic lithium anode. For example, it is possible to substitute the lithium anode by a graphite anode, $\mathrm{Li_xC_6}$, that is likewise to be represented by a many-particle model. In this case our stochastic model can be applied, only the kinetic coefficients and the chemical potentials must be interchanged accordingly. Then simulations of commercial cells become possible.

References

[Baz13] M. Z. Bazant. Theory of chemical kinetics and charge transfer based on nonequilibrium thermodynamics. *Accounts Chem. Res.*, 46(5):1144–1160, 2013.

[BCB11] P. Bai, D.A. Cogswell, and M.Z. Bazant. Suppression of phase separation in $LiFePO_4$ nanoparticles during battery discharge. *Nano Lett.*, 11(11):4890–4896, 2011.

[BD14] D. Bothe and W. Dreyer. Continuum thermodynamics of chemically reacting fluid mixtures. *Acta Mech.*, pages 1–49, 2014.

[Bed86] D. Bedeaux. Nonequilibrium thermodynamics and statistical physics of surfaces. In Prigogine Ilya and S. A. Rice, editors, *Advances in Chemical Physics*, volume 64, pages 47–109. John Wiley Sons, Inc., 1986.

[CA65] R.C. Costen and D. Adamson. Three-dimensional derivation of the electrodynamic jump conditions and momentum-energy laws at a moving boundary. *Proceedings of the IEEE*, 53(9):1181–1196, 1965.

[CEGS+13] W.C. Chueh, F. El Gabaly, J.D. Sugar, N.C. Bartelt, A.H. McDaniel, K.R. Fenton, K.R. Zavadil, T. Tyliszczak, W. Lai, and K.F. McCarty. Intercalation pathway in many-particle LiFePO4 electrode revealed by nanoscale state-of-charge mapping. *Nano Letters*, 13(3):866–872, 2013.

[DBG+05] R. Dominko, M. Bele, M. Gaberšček, M. Remskar, D. Hanzel, S. Pejovnik, and J. Jamnik. Impact of the carbon coating thickness on the electrochemical performance of LiFePO4/C composites. *Journal of The Electrochemical Society*, 152(3):A607–A610, 2005.

[DFG+16] W Dreyer, P.K. Friz, P Gajewski, C. Guhlke, and M. Maurelli. to be published. *WIAS Preprint*, 2016.

[DFN93] M. Doyle, T.F. Fuller, and J. Newman. Modeling of galvanostatic charge and discharge of the lithium/polymer/insertion cell. *Journal of The Electrochemical Society*, 140(6):1526–1533, 1993.

[DG15] W. Dreyer and C. Guhlke. Sharp limit of the viscous Cahn–Hilliard equation and thermodynamic consistency. *Continuum Mech. Thermodyn.*, page 22, 2015.

[DGG+10] W. Dreyer, M. Gaberšček, C. Guhlke, R. Huth, and J. Jamnik. Phase transition in a rechargeable lithium battery. *European Journal of Applied Mathematics*, 22:267–290, 2010.

[DGH11] W. Dreyer, C. Guhlke, and M. Herrmann. Hysteresis and phase transition in many-particle storage systems. *Continuum Mech. Thermodyn.*, 23(3):211–231, 2011.

[DGM13] W. Dreyer, C. Guhlke, and R. Müller. Overcoming the shortcomings of the Nernst–Planck model. *Phys. Chem. Chem. Phys.*, 15:7075–7086, 2013.

[DGM15] W. Dreyer, C. Guhlke, and R. Müller. Modeling of electrochemical double layers in thermodynamic non-equilibrium. *Phys. Chem. Chem. Phys.*, 17:27176–27194, 2015.

[DGM16] W. Dreyer, C. Guhlke, and R. Müller. A new perspective on the electron transfer: recovering the Butler-Volmer equation in non-equilibrium thermodynamics. *Phys. Chem. Chem. Phys.*, 18:24966–24983, 2016.

[DHM+15] W. Dreyer, R. Huth, A. Mielke, J. Rehberg, and M. Winkler. Global existence for a nonlocal and nonlinear Fokker–Planck equation. *Zeitschrift für angewandte Mathematik und Physik*, 66(2):293–315, 2015.

[DJG+10] W. Dreyer, J. Jamnik, C. Guhlke, R. Huth, J. Moškon, and M. Gaberšček. The thermodynamic origin of hysteresis in insertion batteries. *Nature Materials*, 9:448–453, 2010.

[dM63] S. R. deGroot and P. Mazur. *Non-Equilibrium Thermodynamics*. North Holland, Amsterdam, 1963.

[DMC+08] C. Delmas, M. Maccario, L. Croguennec, F. Le Cras, and F. Weill. Lithium deintercalation in $LiFePO_4$ nanoparticles via a domino-cascade model. *Nature Materials*, 7:665–671, 2008.

[DN97] M. Doyle and J. Newman. Analysis of capacity-rate data for lithium batteries using simplified models of the discharge process. *Journal of Applied Electrochemistry*, 27(7):846–856, 1997.

[FD11] M. Farkhondeh and C. Delacourt. Mathematical modeling of commercial LiFePO4 electrodes based on variable solid-state diffusivity. *Journal of The Electrochemical Society*, 159(2):A177–A192, 2011.

[FHM14] N. Fournier, M. Hauray, and S. Mischler. Propagation of chaos for the 2D viscous vortex model. *J. Eur. Math. Soc. (JEMS)*, 16(7):1423–1466, 2014.

[Fra13] A.A. Franco. Multiscale modelling and numerical simulation of rechargeable lithium ion batteries: concepts, methods and challenges. *RSC Advances*, 3:13027–13058, 2013.

[FSP+14] M. Farkhondeh, M. Safari, M. Pritzker, M. Fowler, Taeyoung Han, Jasmine Wang, and C. Delacourt. Full-range simulation of a commercial LiFePO4 electrode accounting for bulk and surface effects: A comparative analysis. *Journal of The Electrochemical Society*, 161(3):A201–A212, 2014.

[Gar96] C.W. Gardiner. *Handbook of Stochastic Methods for Physics, Chemistry and the Natural Sciences*. Springer Series in Synergetics Springer-Verlag, 1996.

[Guh15] C. Guhlke. *Theorie der elektrochemischen Grenzfläche*. PhD thesis, TU-Berlin, 2015.

[HNV12] M. Herrmann, B. Niethammer, and J.J.L. Velázquez. Kramers and non-kramers phase transitions in many-particle systems with dynamical constraint. *SIAM Multiscale Model. Simul.*, 10(3):818–852, 2012.

[HNV14] M. Herrmann, B. Niethammer, and J.J.L. Velázquez. Rate-independent dynamics and Kramers-type phase transitions in nonlocal Fokker-Planck equations with dynamical control. *Arch. Ration. Mech. Anal.*, 124(3):803–866, 2014.

[HSB11] C. Hellwig, S. Sörgel, and W.G. Bessler. A multi-scale electrochemical and thermal model of a LiFePO4 battery. *ECS Transactions*, 35(32):215–228, 2011.

[KR16] C. Kraus and A. Roggensack. Existence of weak solutions for the Cahn–Hilliard reaction model including elastic effects and damage. *WIAS Preprint*, 2231, 2016.

[LEGF+14] Y. Li, F. El Gabaly, T.R. Ferguson, R.B. Smith, N.C. Bartelt, J.D. Sugar, K.R. Fenton, D.A. Cogswell, A.L.D. Kilcoyne, T. Tyliszczak, M.Z. Bazant, and W.C. Chueh. Current-induced transition from particle-by-particle to concurrent intercalation in phase-separating battery electrodes. *Nature Materials*, 13:1476–1122, 2014.

[LML+15] Y. Li, S. Meyer, J. Lim, S.C. Lee, W.E. Gent, S. Marchesini, H. Krishnan, T. Tyliszczak, D. Shapiro, A.L.D. Kilcoyne, and W.C. Chueh. Effects of particle size, electronic connectivity, and incoherent nanoscale domains on the sequence of lithiation in LiFePO4 porous electrodes. *Advanced Materials*, 27(42):6591–6597, 2015.

[LWG+15] Y. Li, J.N. Weker, W.E. Gent, D.N. Mueller, J. Lim, D.A. Cogswell, T. Tyliszczak, and W.C. Chueh. Dichotomy in the lithiation pathway of ellipsoidal and platelet LiFePO4 particles revealed through nanoscale operando state-of-charge imaging. *Advanced Functional Materials*, 25(24):3677–3687, 2015.

[LZ11] A. Latz and J. Zausch. Thermodynamic consistent transport theory of Li-ion batteries. *J. Power Sources*, 196(6):3296–3302, 2011.

[LZ13] A. Latz and J. Zausch. Thermodynamic derivation of a Butler Volmer model for intercalation in Li-ion batteries. *Electrochim. Acta*, 2013.

[MDCK+07] J. Moskon, R. Dominko, R. Cerc-Korosec, M. Gaberšček, and J. Jamnik. Morphology and electrical properties of conductive carbon coatings for cathode materials. *J. Power Sources*, 174(2):683–688, 2007.

[MR59] J. Meixner and H. G. Reik. *Thermodynamik der irreversiblen Prozesse*, volume 3, pages 413–523. Springer, Berlin, 1959.

[Mül85] I. Müller. *Thermodynamics, Interaction of Mechanics and Mathematics Series*. Pitman Advanced Publishing Program, Boston, 1985.

[PNG97] A.K. Padhi, K.S. Nanjundaswamy, and J.B. Goodenough. Phospho-olivines as positive-electrode materials for rechargeable lithium batteries. *J. Electrochem. Soc.*, 144:1188–1194, 1997.

[SCB08] G.K. Singh, G. Ceder, and M.Z. Bazant. Intercalation dynamics in rechargeable battery materials: General theory and phase-transformation waves in LiFePO4. *Electrochimica Acta*, 53(26):7599 – 7613, 2008.

[SD11] M. Safari and C. Delacourt. Mathematical modeling of lithium iron phosphate electrode: Galvanostatic charge/discharge and path dependence. *Journal of The Electrochemical Society*, 158(2):A63–A73, 2011.

[SN04] V. Srinivasan and J. Newman. Discharge model for the lithium iron-phosphate electrode. *Journal of The Electrochemical Society*, 151(10):A1517–A1529, 2004.

[Szn91] A.-S. Sznitman. Topics in propagation of chaos. In *École d'Été de Probabilités de Saint-Flour XIX—1989*, volume 1464 of *Lecture Notes in Math.*, pages 165–251. Springer, Berlin, 1991.

[ZB14] Y. Zeng and M.Z. Bazant. Phase separation dynamics in isotropic ion-intercalation particles. *SIAM J. Appl. Math.*, 74(4):980–1004, 2014.